Electronic Supplementary Material (ESI) for Nanoscale.

Synthesis of octahedral, truncated octahedral, and cubic Rh_2Ni nanocrystals and their structure–activity relationship for decomposition of hydrazine in aqueous solution to hydrogen

Chun Li,[a, b] Tao Wang,[a, b] Wei Chu,*[c] Ping Wu,[a, b] and Dong Ge Tong*[a, b]

[a] Mineral Resources Chemistry Key Laboratory of Sichuan Higher Education Institutions, College of Materials and Chemistry & Chemical Engineering, Chengdu University of Technology, Chengdu 610059, China.

E-mail: tongdongge@163.com; Fax: +86 28 8407 9074

[b] Collaborative Innovation Center of Panxi Strategic Mineral Resources Multi-purpose Utilization, Chengdu 610059, China.

[c] College of Chemical Engineering and Key Laboratory of Green Chemistry & Technology of Ministry of Education, Sichuan University, Chengdu 610065, China.

E-mail: chuwei1965@foxmail.com; Fax: +86 28 8540 3397

Summary: 42 Pages; 4 Tables; 50 Figures

Table S1 The effect of reaction parameters, including reaction temperature, reaction time, Rh/Ni precursors, margaric acid/(Rh + Ni), BTM/(Rh + Ni), $Ge(C_2H_5)_4$/(Rh + Ni) molar ratios on the octahedrons percentage, average size, and chemical composition of Rh_2Ni nanooctahedrons.

Sample	Reaction temperature / °C	Reaction time / min	Rh/Ni precursors	margaric acid/(Rh + Ni)	BTM/(Rh + Ni)	$Ge(C_2H_5)_4$/(Rh + Ni)	Octahedrons percentage / %	Average size / nm	Chemical composition	Rh/Ni atomic ratio
1	200	45	1:1	1:1	1.2	0.1	100.0	16.8	$Rh_{66.79}Ni_{33.21}$	2.01
2	190	45	1:1	1:1	1.2	0.1	100.0	12.9	$Rh_{66.67}Ni_{33.33}$	2.00
3	180	45	1:1	1:1	1.2	0.1	100.0	8.6	$Rh_{66.68}Ni_{33.32}$	2.00
4	170	45	1:1	1:1	1.2	0.1	84.1	7.3	$Rh_{68.05}Ni_{31.95}$	2.13
5	160	45	1:1	1:1	1.2	0.1	67.2	5.9	$Rh_{70.04}Ni_{29.76}$	2.36
6	140	45	1:1	1:1	1.2	0.1	55.7	4.4	$Rh_{73.47}Ni_{29.53}$	2.77
7	180	30	1:1	1:1	1.2	0.1	40.0	3.2	$Rh_{63.24}Ni_{36.76}$	1.72
8	180	90	1:1	1:1	1.2	0.1	100.0	8.8	$Rh_{66.78}Ni_{33.22}$	2.01
9	180	45	1:1	2:1	1.2	0.1	100.0	8.6	$Rh_{66.89}Ni_{33.11}$	2.02
10	180	45	1:1	1:2	1.2	0.1	95.0	11.2	$Rh_{67.53}Ni_{32.47}$	2.08
11	180	45	1:1	1:3	1.2	0.1	40.0	13.0	$Rh_{69.42}Ni_{30.58}$	2.27
12	180	45	1:1	1:4	1.2	0.1	20.0	13.0	$Rh_{71.75}Ni_{28.25}$	2.54
13	180	45	2:1	1:1	1.2	0.1	95.7	9.6	$Rh_{67.00}Ni_{33.00}$	2.03
14	180	45	1:2	1:1	1.2	0.1	84.5	8.0	$Rh_{67.85}Ni_{32.15}$	2.11
15	180	45	1:1	1:1	1.3	0.1	88.9	7.4	$Rh_{67.32}Ni_{32.68}$	2.06
16	180	45	1:1	1:1	1.1	0.1	63.4	9.1	$Rh_{67.01}Ni_{32.99}$	2.03
17	180	45	1:1	1:1	1.0	0.1	45.8	10.8	$Rh_{67.43}Ni_{32.57}$	2.07
18	180	45	1:1	1:1	1.2	0.125	100	8.6	$Rh_{66.69}Ni_{33.31}$	2.00
19	180	45	1:1	1:1	1.2	0.05	98.5	11.3	$Rh_{66.68}Ni_{33.32}$	2.00
20	180	45	1:1	1:1	1.2	0.033	97.1	13.8	$Rh_{66.67}Ni_{33.33}$	2.00
21	180	45	1:1	1:1	1.2	0.025	95.6	16.7	$Rh_{66.71}Ni_{33.29}$	2.00

Table S2 The effect of reaction parameters, including reaction temperature, reaction time, Rh/Ni precursors, margaric acid/1-aminoheptadecane, BTM/(Rh + Ni), $Ge(C_2H_5)_4$ /(Rh + Ni) molar ratios on the truncated octahedrons percentage, average size, and chemical composition of Rh_2Ni truncated nanooctahedrons.

Sample	Reaction temperature / °C	Reaction time / min	Rh/Ni precursors	margaric acid / 1-aminoheptadecane	BTM/(Rh + Ni)	$Ge(C_2H_5)_4$ /(Rh + Ni)	truncated nanooctahedrons percentage / %	average size / nm	Chemical composition	Rh/Ni atomic ratio
1	200	45	1:1	1:1	1.2	0.1	100.0	15.7	$Rh_{66.67}Ni_{33.33}$	2.00
2	190	45	1:1	1:1	1.2	0.1	100.0	12.4	$Rh_{66.79}Ni_{33.21}$	2.01
3	180	45	1:1	1:1	1.2	0.1	100.0	8.7	$Rh_{66.71}Ni_{33.29}$	2.00
4	170	45	1:1	1:1	1.2	0.1	81.4	7.3	$Rh_{66.74}Ni_{33.26}$	2.10
5	160	45	1:1	1:1	1.2	0.1	65.6	5.7	$Rh_{66.70}Ni_{33.30}$	2.30
6	140	45	1:1	1:1	1.2	0.1	52.5	4.8	$Rh_{66.70}Ni_{27.10}$	2.69
7	180	30	1:1	1:1	1.2	0.1	43.1	11.8	$Rh_{63.90}Ni_{36.10}$	1.77
8	180	90	1:1	1:1	1.2	0.1	100.0	8.6	$Rh_{67.00}Ni_{33.00}$	2.03
9	180	45	1:1	2:1	1.2	0.1	50.0	9.7	$Rh_{66.69}Ni_{33.31}$	2.00
10	180	45	1:1	1:2	1.2	0.1	4**8.**9	11.0	$Rh_{68.94}Ni_{31.06}$	2.22
11	180	45	2:1	1:1	1.2	0.1	93.2	9.2	$Rh_{66.78}Ni_{33.22}$	2.01
12	180	45	1:2	1:1	1.2	0.1	81.3	7.9	$Rh_{68.15}Ni_{31.85}$	2.14
13	180	45	1:1	1:1	1.3	0.1	84.2	7.1	$Rh_{67.23}Ni_{32.77}$	2.05
14	180	45	1:1	1:1	1.1	0.1	66.1	8.6	$Rh_{66.68}Ni_{33.32}$	2.00
15	180	45	1:1	1:1	1.0	0.1	42.3	10.4	$Rh_{67.74}Ni_{32.26}$	2.10
16	180	45	1:1	1:1	1.2	0.125	100.0	8.7	$Rh_{66.79}Ni_{33.21}$	2.01
17	180	45	1:1	1:1	1.2	0.05	96.2	10.8	$Rh_{66.67}Ni_{33.33}$	2.00
18	180	45	1:1	1:1	1.2	0.033	94.2	13.1	$Rh_{66.89}Ni_{33.11}$	2.02
19	180	45	1:1	1:1	1.2	0.025	92.3	15.4	$Rh_{66.67}Ni_{33.33}$	2.00

Table S3 The effect of reaction parameters, including reaction temperature, reaction time, Rh/Ni precursors, 1-aminoheptadecane/(Rh + Ni), BTM/(Rh + Ni), $Ge(C_2H_5)_4$/(Rh + Ni) molar ratios on the cubes percentage, average size, and chemical composition of Rh_2Ni nanocubes.

Sample	Reaction temperature / °C	Reaction time / min	Rh/Ni precursors	1-aminoheptadecane /(Rh + Ni)	BTM/(Rh + Ni)	$Ge(C_2H_5)_4$ /(Rh + Ni)	Cubes percentage / %	average size / nm	Chemical composition	Rh/Ni atomic ratio
1	200	45	1:1	1:1	1.2	0.1	100.0	13.8	$Rh_{66.71}Ni_{33.29}$	2.00
2	190	45	1:1	1:1	1.2	0.1	100.0	11.0	$Rh_{66.67}Ni_{33.33}$	2.00
3	180	45	1:1	1:1	1.2	0.1	100.0	8.5	$Rh_{66.69}Ni_{33.31}$	2.00
4	170	45	1:1	1:1	1.2	0.1	78.4	6.2	$Rh_{66.64}Ni_{33.36}$	2.09
5	160	45	1:1	1:1	1.2	0.1	63.5	5.3	$Rh_{66.04}Ni_{33.96}$	2.23
6	140	45	1:1	1:1	1.2	0.1	52.1	3.6	$Rh_{72.30}Ni_{27.70}$	2.61
7	180	30	1:1	1:1	1.2	0.1	43.4	2.5	$Rh_{62.69}Ni_{37.31}$	1.68
8	180	90	1:1	1:1	1.2	0.1	90.0	9.8	$Rh_{67.00}Ni_{33.00}$	2.03
9	180	45	1:1	2:1	1.2	0.1	100.0	8.7	$Rh_{66.68}Ni_{33.32}$	2.00
10	180	45	1:1	1:2	1.2	0.1	97.0	9.8	$Rh_{68.94}Ni_{31.06}$	2.22
11	180	45	1:1	1:3	1.2	0.1	43.2	11.2	$Rh_{70.59}Ni_{29.41}$	2.40
12	180	45	1:1	1:4	1.2	0.1	17.2	13.0	$Rh_{71.75}Ni_{28.25}$	2.54
13	180	45	2:1	1:1	1.2	0.1	92.7	8.9	$Rh_{67.23}Ni_{32.77}$	2.05
14	180	45	1:2	1:1	1.2	0.1	82.3	6.7	$Rh_{68.25}Ni_{31.75}$	2.15
15	180	45	1:1	1:1	1.3	0.1	89.4	6.4	$Rh_{67.11}Ni_{32.89}$	2.04
16	180	45	1:1	1:1	1.1	0.1	61.9	7.6	$Rh_{66.79}Ni_{33.21}$	2.01
17	180	45	1:1	1:1	1.0	0.1	47.0	8.9	$Rh_{67.64}Ni_{32.36}$	2.09
18	180	45	1:1	1:1	1.2	0.125	100.0	8.7	$Rh_{66.89}Ni_{33.11}$	2.02
19	180	45	1:1	1:1	1.2	0.05	93.2	9.8	$Rh_{66.44}Ni_{33.56}$	1.98
20	180	45	1:1	1:1	1.2	0.033	91.1	12.3	$Rh_{66.69}Ni_{33.31}$	2.00
21	180	45	1:1	1:1	1.2	0.025	89.2	13.9	$Rh_{66.56}Ni_{33.44}$	1.99

Table S4 Catalytic performance of different catalysts for decomposition of hydrazine in aqueous solution to produce H_2

Samples	Temperature / K	H_2 generation volume / mL	H_2 selectivity / %	Time / min	TOF / min^{-1}	TTON	ATOF / min^{-1}
Rh_2Ni nanooctahedrons/C in this work	293	2195.2	100.0	21	15.7	27, 723	15.4
Rh_2Ni truncated nanooctahedrons/C in this work	293	2041.5	93.0	31	10.6	-	-
Rh_2Ni nanocubes/C in this work	293	1756.6	80.0	54	6.1	-	-
$Rh_{58}Ni_{42}$@MIL-101 [40]	323	141.4	100.0	7	5.73	-	-
Rh-Cu nanoframe [73]	298	44.8	31.4	300	0.56		
In situ RhNiB [39]	298	89.6	100.0	22	-	-	-
Rh/Ni@SiO_2 [30]	298	91.7	99.4	90	1.1	-	-
In situ Rh_4Ni [8]	298	89.6	100.0	160	0.25	-	-
In situ $Rh_{4.69}Ni$/graphene [15]	298	89.6	100.0	49	1.91	-	-
$Ni_{64}Pt_{36}$/MIL-96 [29]	298	141.4	100.0	12	1.91		
$Ni_{88}Pt_{12}$@MIL-101 [31]	298	87.8	100.0	42	1.09	-	-
$Ni_{87}Pt_{13}$/meso-Al_2O_3 [43]	323	89.6	100.0	5	2.67		
In situ $Ni_{0.93}Pt_{0.07}$ [9]	298	89.6	100.0	190	0.0021	-	-
$NiPt_{0.057}/Al_2O_3$ [21]	303	70.2	98.0	11.5	0.28	-	-
Amorphous $Ni_{0.9}Pt_{0.1}/Ce_2O_3$ [25]	298	172.0	100.0	43	0.47	-	-
In situ $Ni_{0.95}Ir_{0.05}$ [27]	298	89.6	100.0	390	0.26	-	-
$Pt_{0.6}Ni_{0.4}$/PDA–Rgo[46]	293	-	100.0	3.5	11.43	-	-
$Ni_{84}Pt_{16}$/graphene[47]	298	87.8	100.0	42	2.22	-	-
Ni@NiePt/La_2O_3[48]	323	-	100.0	2.6	5.20	-	-
$Ni_{85}Ir_{15}$@MIL-101[45]	298	-	100.0	-	0.4		
In situ $Ni_{0.6}Pd_{0.4}$ [14]	298	71.7	80.0	300	-	-	-
NiFe [13]	298	89.6	100.0	190	-	-	-
Ni-Al_2O_3-HT [16]	303	-	93.0	70	0.033	-	-

Ni-0.080CeO_2 [44]	323	71.7	99.0	10	0.86		
$NiIr_{0.059}/Al_2O_3$ [27]	303		99.0	12.5	0.21	-	-
Mondispersed Ni_3Fe nanospheres /C [22]	293	224.0	100.0	27	9.26	15840	8.8
NiMoB-La$(OH)_3$ [24]	323	136.0	100.0	15	0.24	-	-
$Ni_{0.6}Fe_{0.4}Mo$ [42]	323	89.6	100.0	15	0.48	-	-
$Ni_{30}Fe_{30}Pd_{40}$ [49]	323	224.0	100.0	27	0.36	-	-
Co-B honeycomb [21]	298	1872.6	41.8	13	12.6	18360	10.2
Co-B nanospheres [11]	298	954.2	21.3	23	5.34	-	-
$CoB_{0.358}N_{0.286}H_{0.251}$ nanowires [36]	293	2240.0	100.0	17	76.0	133020	73.9
9.86wt.%Fe-B/WCNTs [23]	298	4345.6	97.0	15.2	67.2	114480	63.6

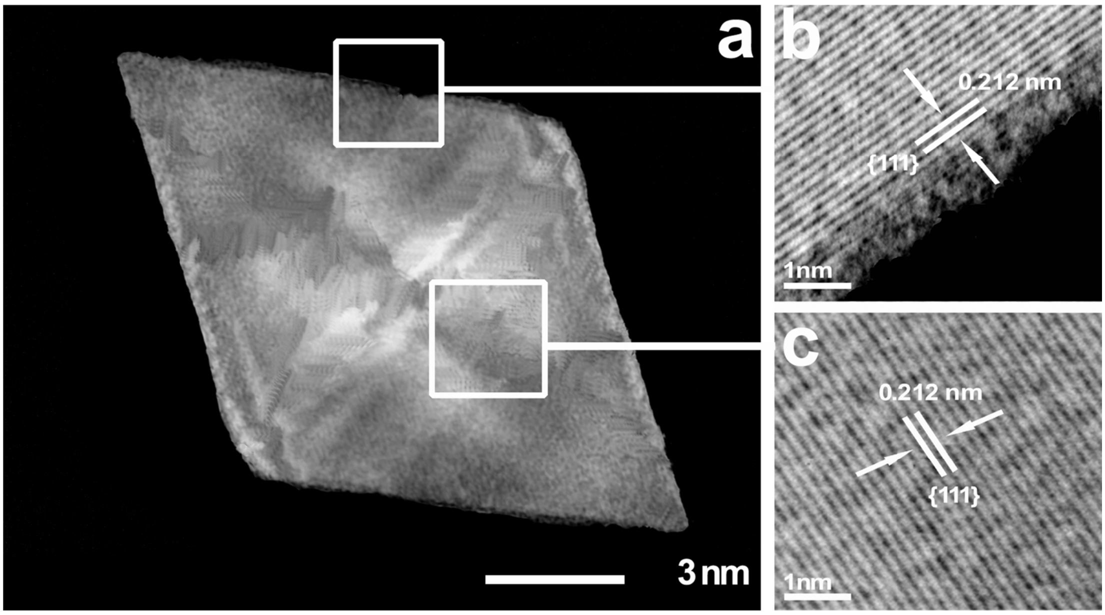

Figure S1. (a)The high resolution STEM (HR-STEM) image of a single Rh_2Ni nanooctahedron; (b, c) Corresponding HR-STEM images of the regions marked in (a).

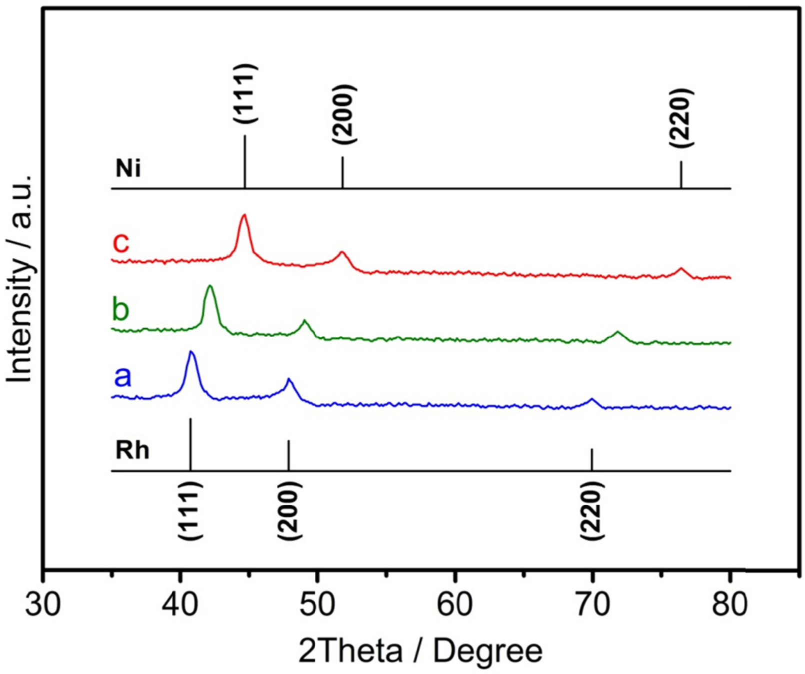

Figure S2. The XRD patterns of the as-prepared (a) Rh nano-octahedrons; (b) Rh_2Ni nano-octahedrons; (c) Ni nano-octahedrons.

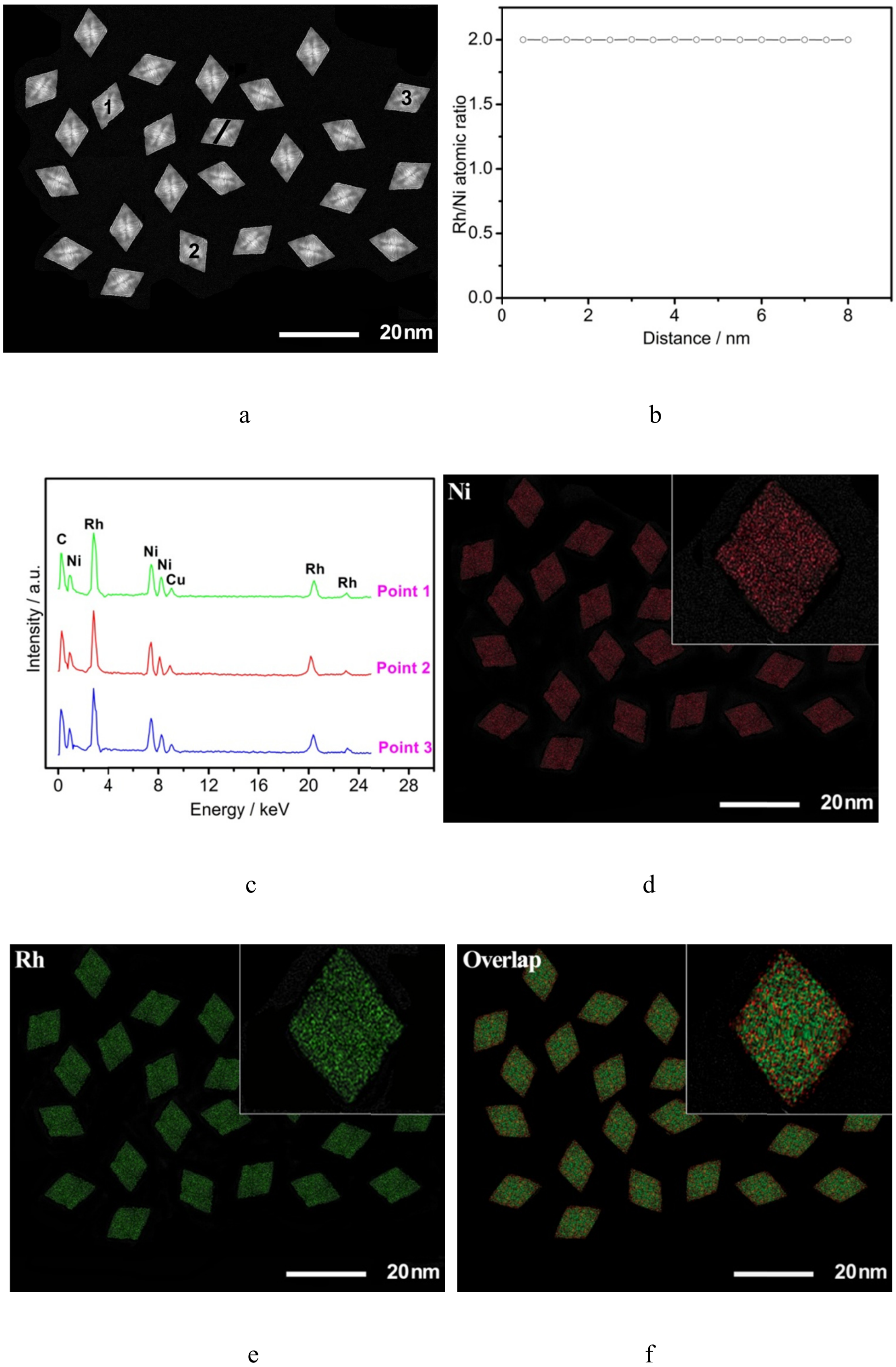

Figure S3. (a) The high-angle annular dark-field scanning transmission electron microscopy (HAADF-STEM); (b) Rh/Ni atomic ratios recorded along the white cross-sectional compositional line shown in (a); (c) the Energy-dispersive X-ray spectroscopy (EDS) at points 1-3 in (a); (d)-(f)the elemental maps of the as-prepared Rh_2Ni nano-octahedrons

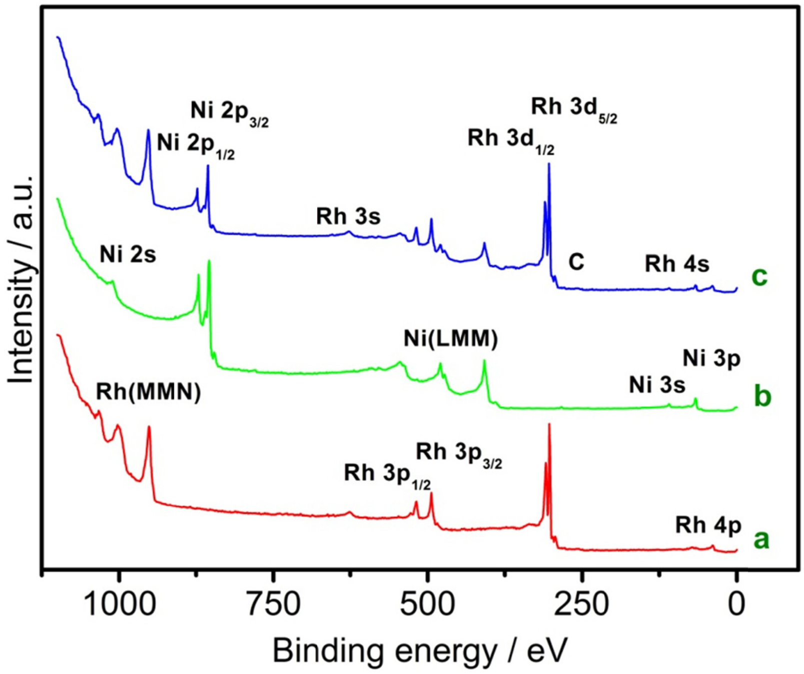

Figure S4. *In-situ* overall XPS spectra of (a) Rh, (b) Ni and (c) the as-prepared Rh_2Ni nano-octahedrons in this work.

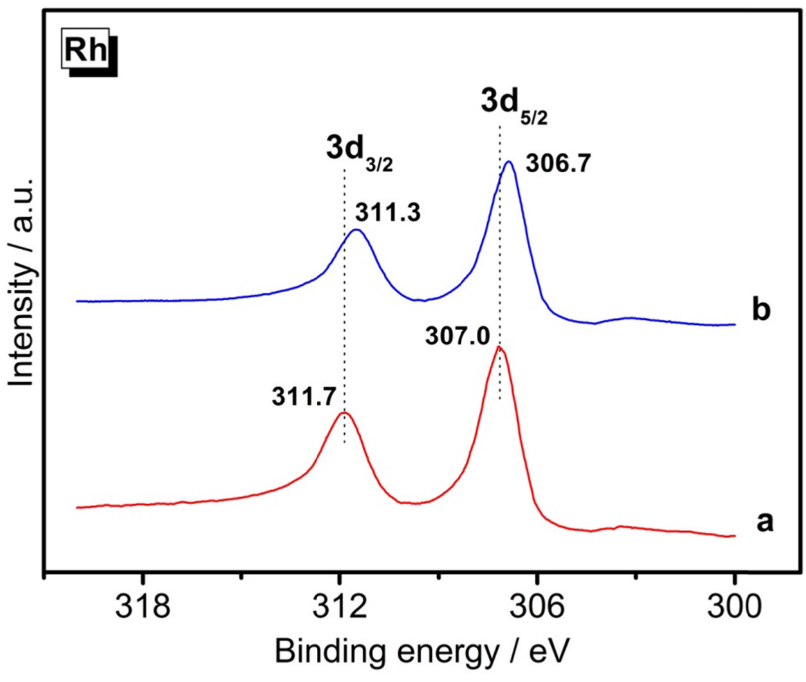

Figure S5. *In-situ* Rh3d XPS spectra of (a) Rh and (b) the as-prepared Rh_2Ni nanooctahedrons in this work.

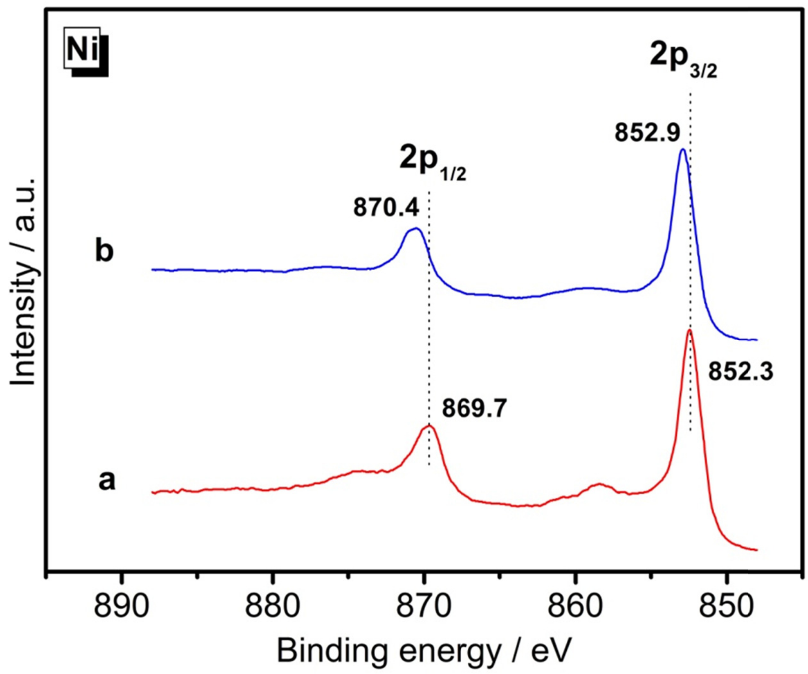

Figure S6. *In-situ* Ni2p XPS spectra of (a) Ni and (b) the as-prepared Rh_2Ni nanooctahedrons in this work.

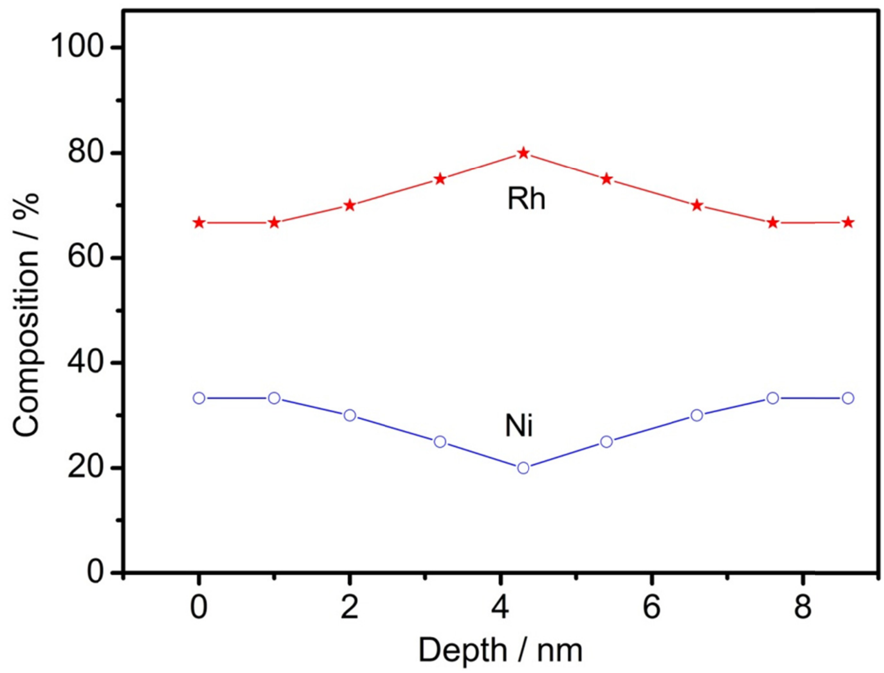

Figure S7. Depth profile curves obtained using X-ray photoelectron spectroscopy of the as-prepared Rh_2Ni nanooctahedrons in this work.

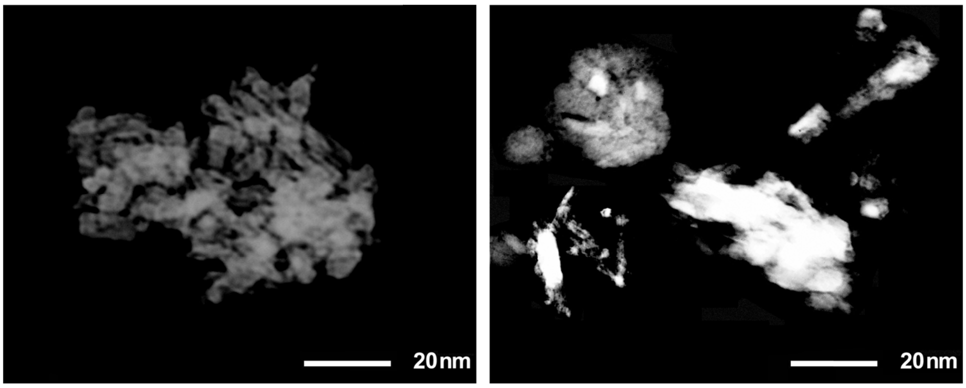

(a) (b)

Figure S8. STEM images of the as-prepared Rh_2Ni: (a) without $Ge(C_2H_5)_4$; (b) without margaric acid

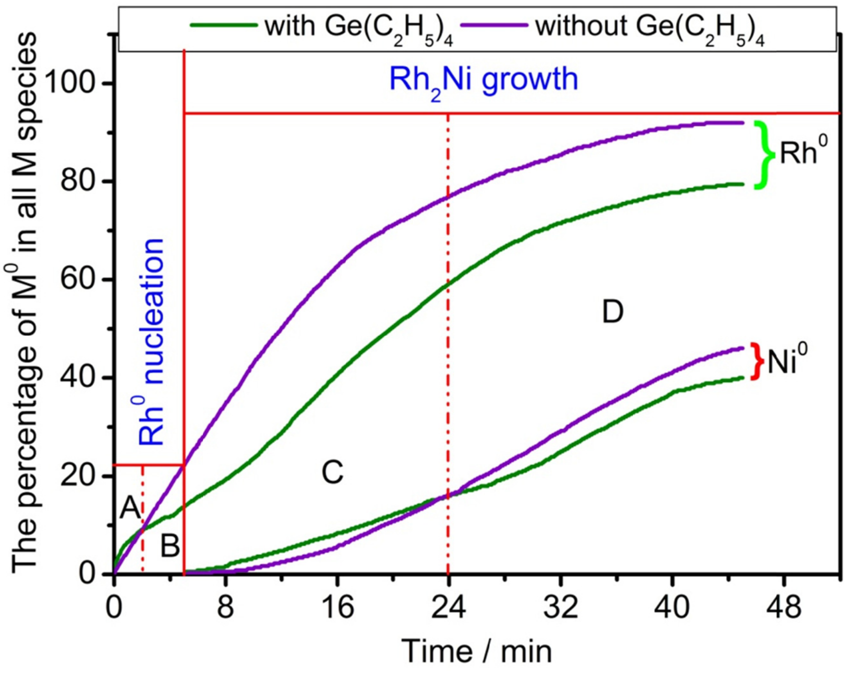

Figure S9. The Rh^0 and Ni^0 percentage in all Rh and Ni species obtained from the *in-situ* XPS measurement during the preparation process of Rh_2Ni NCs with or without the presence of $Ge(C_2H_5)_4$, respectively.

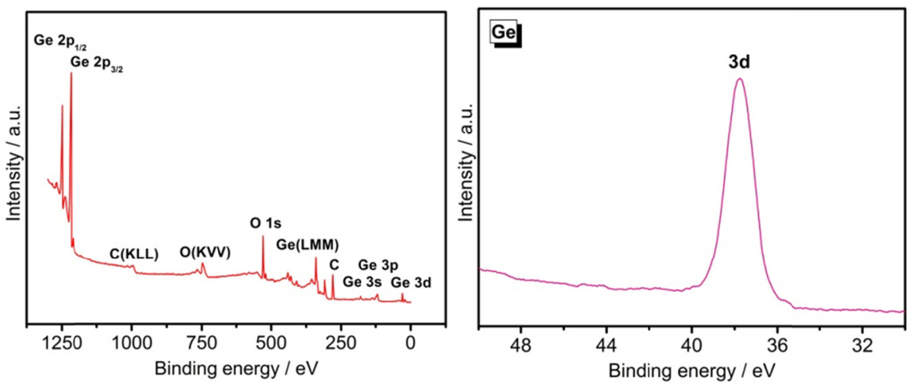

(a) (b)

Figure S10. (a) Overall XPS spectrum and (b) Ge 3d spectrum for the reaction residue after the preparation of Rh_2Ni nanooctahedrons.

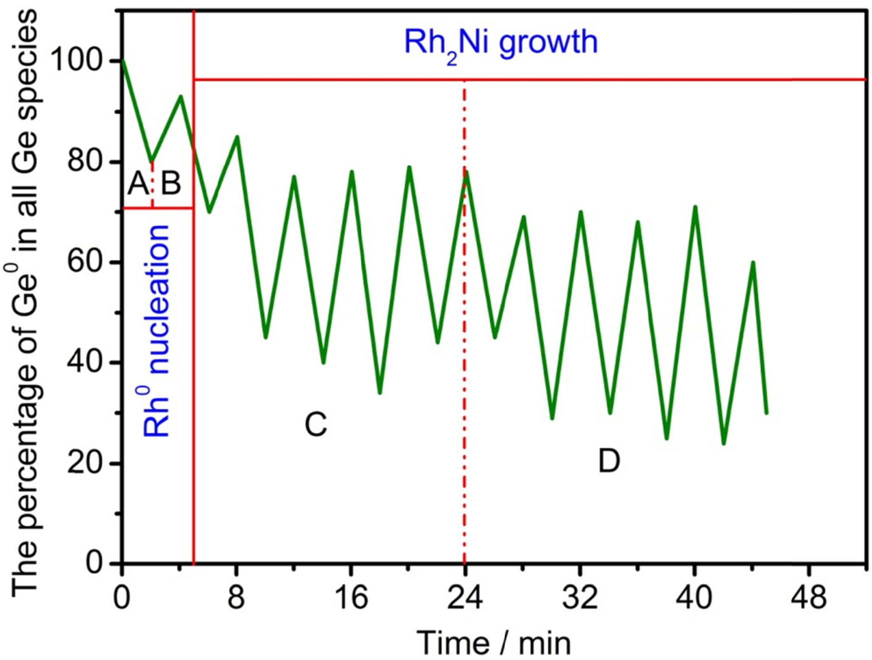

Figure S11. The Ge^0 percentage in all Ge species obtained from the *in-situ* XPS measurement during the preparation process of Rh_2Ni NCs.

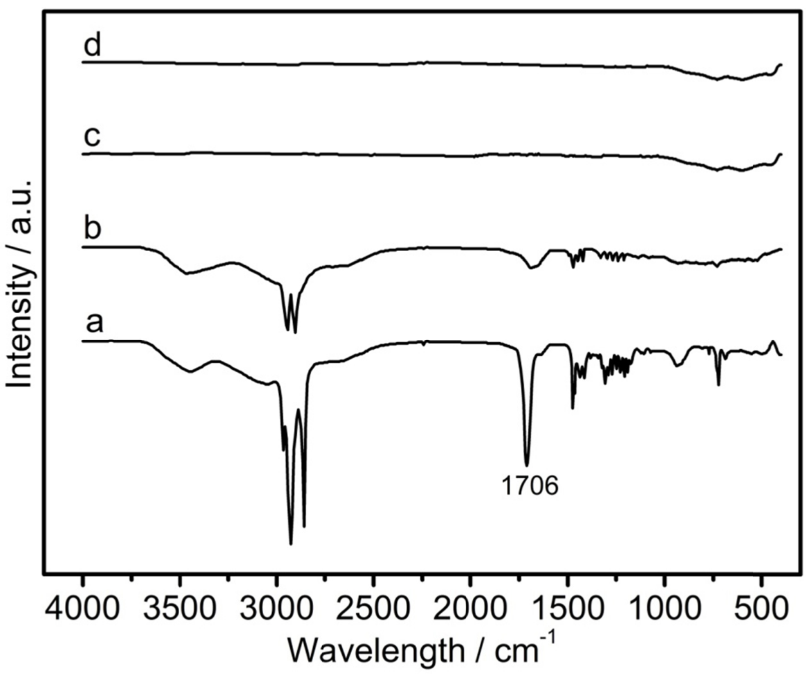

Figure S12. FT-IR spectra of (a) margaric acid; (b) the as-prepared Rh_2Ni nanooctahedrons only washed with water; (c) the as-prepared Rh_2Ni nanooctahedrons washed with ethanol; and (d) commercial Rh_2Ni NPs.

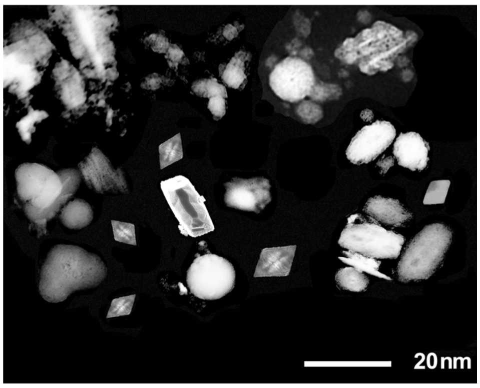

(a)

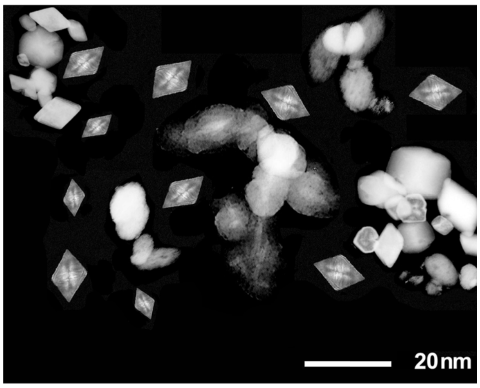

(b)

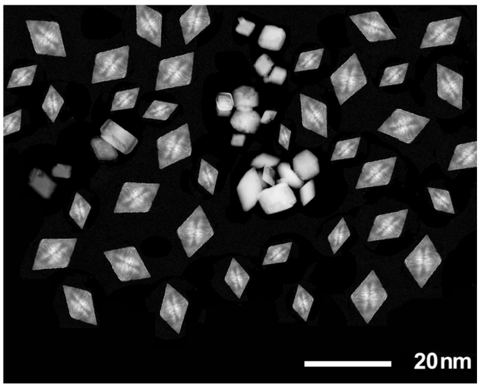

(c)

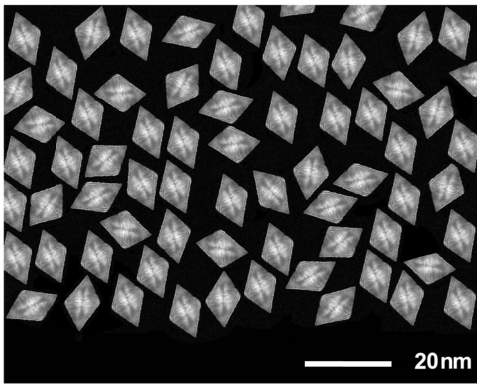

(d)

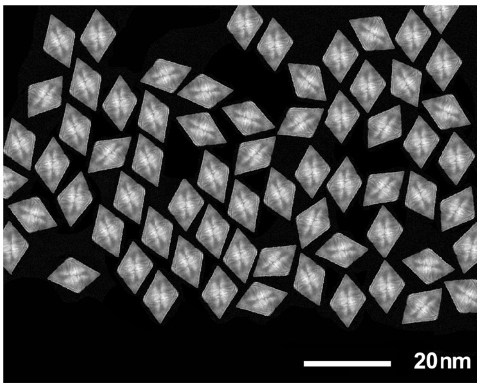

(e)

Figure S13. STEM images of Rh_2Ni synthesized by varying the amounts of margaric acid: (a) 0.01 mmol; (b) 0.025 mmol,, (c) 0.05 mmol, (d) 0.075 mmol and (d) 0.1 mmol, respectively.

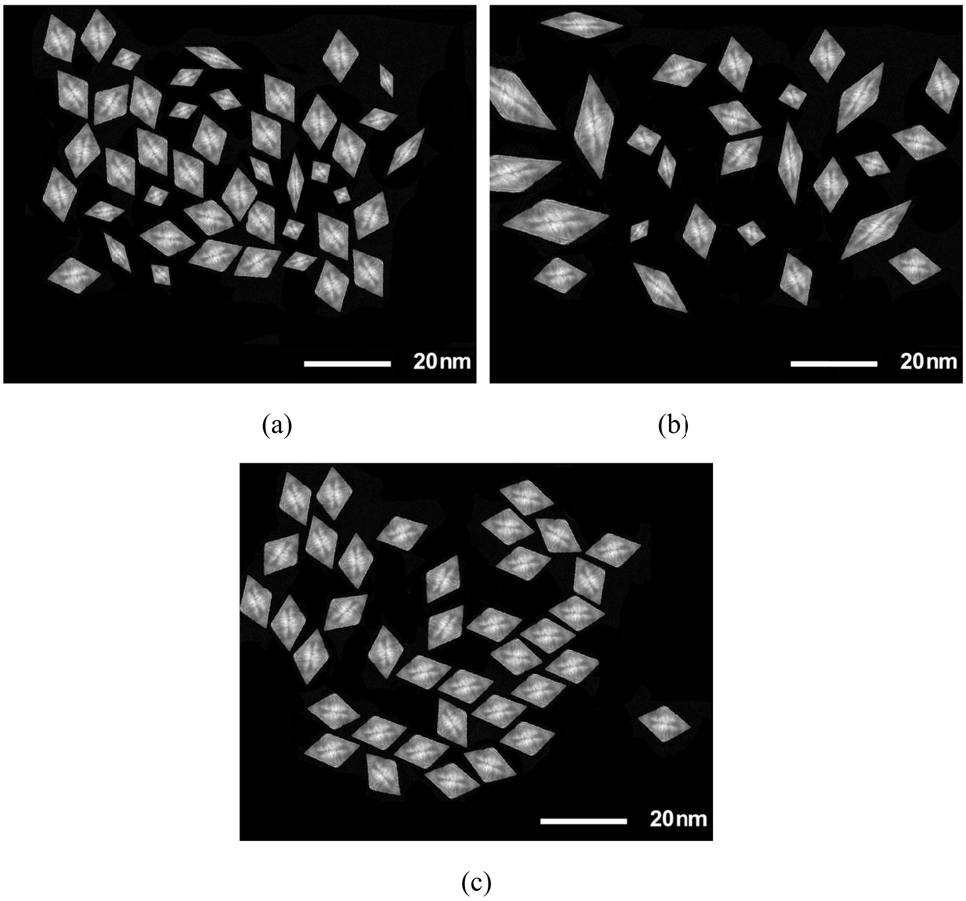

Figure S14. **S**TEM images of the Rh_2Ni NCs prepared using (a) $Ni(acac)_2$; (b) NiC_2O_4 and (c) $NiCl_2$ as the iron precursor.

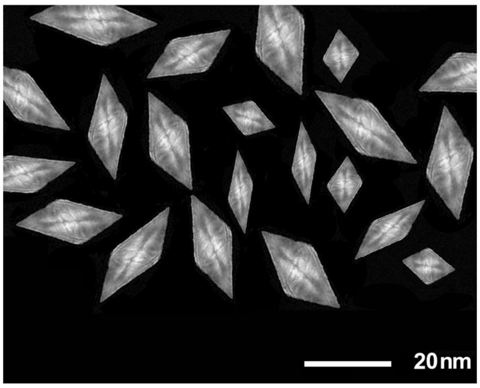

(a)

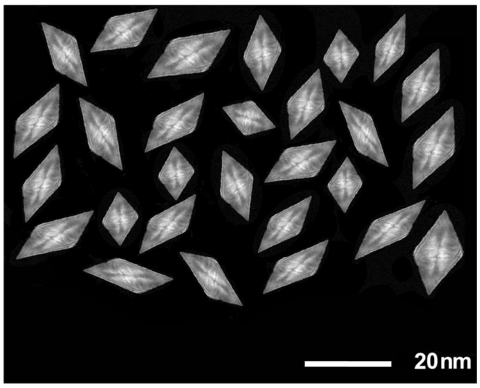

(b)

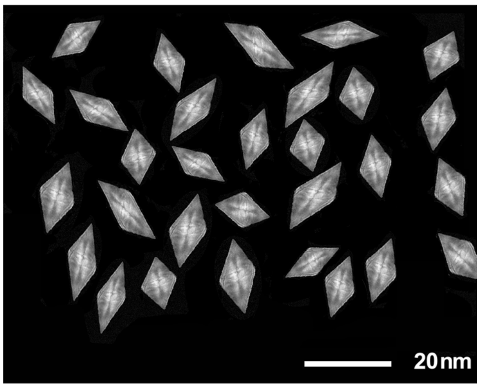

(c)

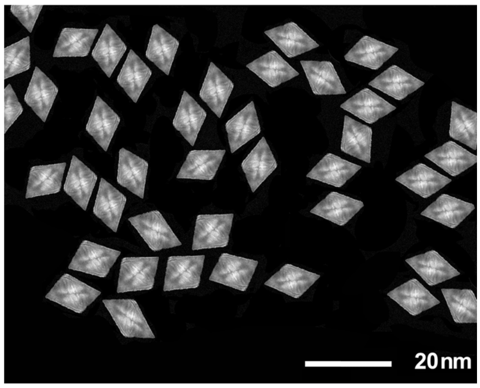

(d)

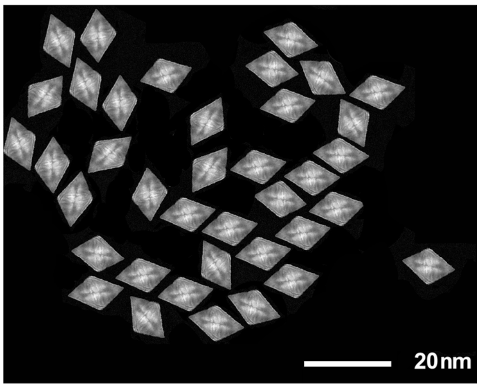

(e)

Figure S15. STEM images of the Rh_2Ni NCs synthesized by varying the molar ratio of $Ge(C_2H_5)_4$/(Rh + Ni)= (a)1:40, (b)1:30, (c)1:20 , (d)1:10 and (e)1:8, respectively.

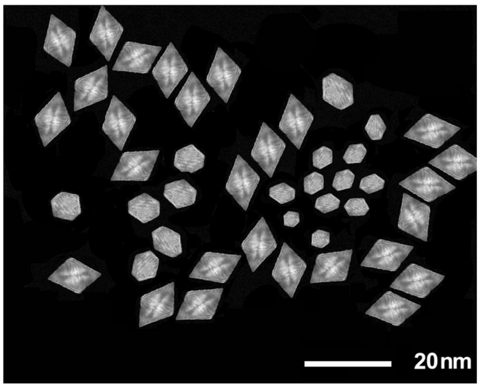

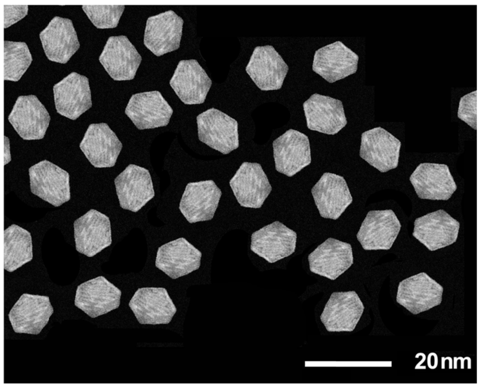

(a) (b)

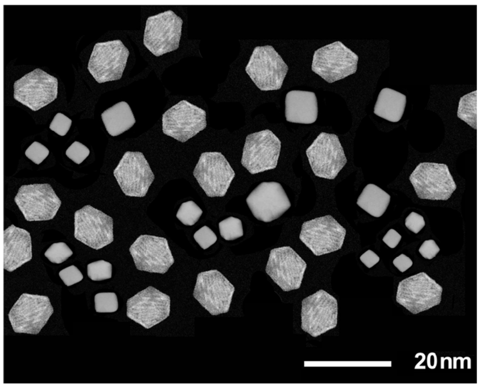

(c)

Figure S16. STEM images of Rh_2Ni synthesized by varying the molar ratio of margaric acid /1-aminoheptadecane : (a) 2, (b) 1, (c) 0.5, respectively.

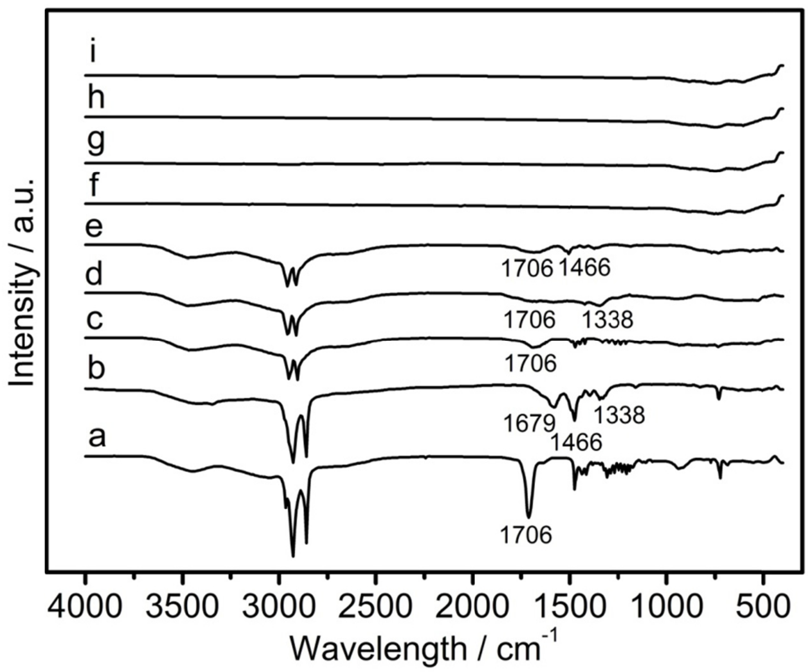

Figure S17. FT-IR spectra of (a) margaric acid; (b) 1-aminoheptadecane; (c) the as-prepared Rh_2Ni nanooctahedrons with the molar ratio of 2 for margaric acid /1-aminoheptadecane only washed with water; (d) the as-prepared Rh_2Ni nanooctahedrons with the molar ratio of 1 for margaric acid /1-aminoheptadecane only washed with water; (e) the as-prepared Rh_2Ni nanooctahedrons with the molar ratio of 0.5 for margaric acid /1-aminoheptadecane only washed with water; (f) the as-prepared Rh_2Ni nanooctahedrons with the molar ratio of 2 for margaric acid /1-aminoheptadecane washed with ethanol; (g) the as-prepared Rh_2Ni nanooctahedrons with the molar ratio of 1 for margaric acid /1-aminoheptadecane washed with ethanol; (h) the as-prepared Rh_2Ni nanooctahedrons with the molar ratio of 0.5 for margaric acid /1-aminoheptadecane washed with ethanol; and (i) commercial Rh_2Ni NPs.

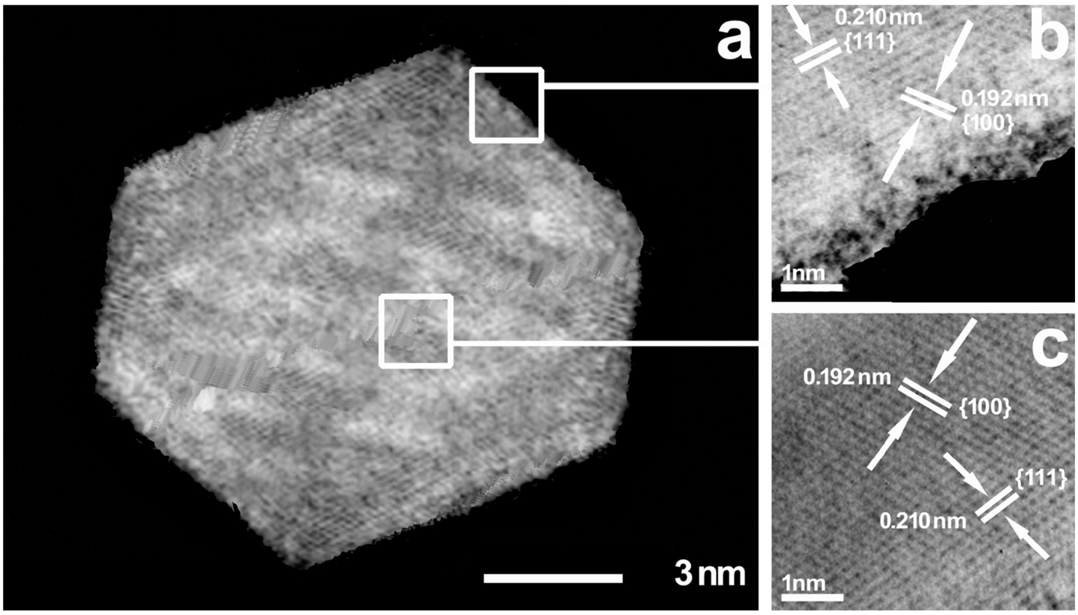

Figure S18. (a)The high resolution STEM (HR-STEM) image of a single Rh_2Ni trunked nanooctahedron; (b, c) Corresponding HR-STEM images of the regions marked in (a).

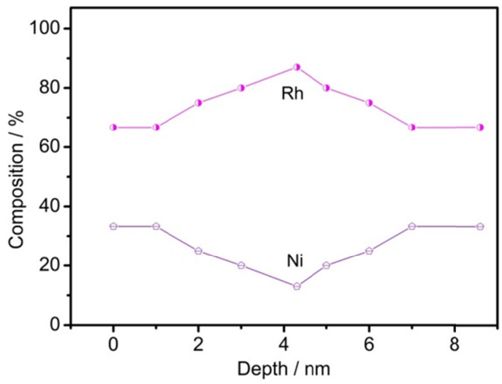

Figure S19. XPS Depth profile curves obtained using X-ray photoelectron spectroscopy of the as-prepared Rh_2Ni trunked nanooctahedrons in this work.

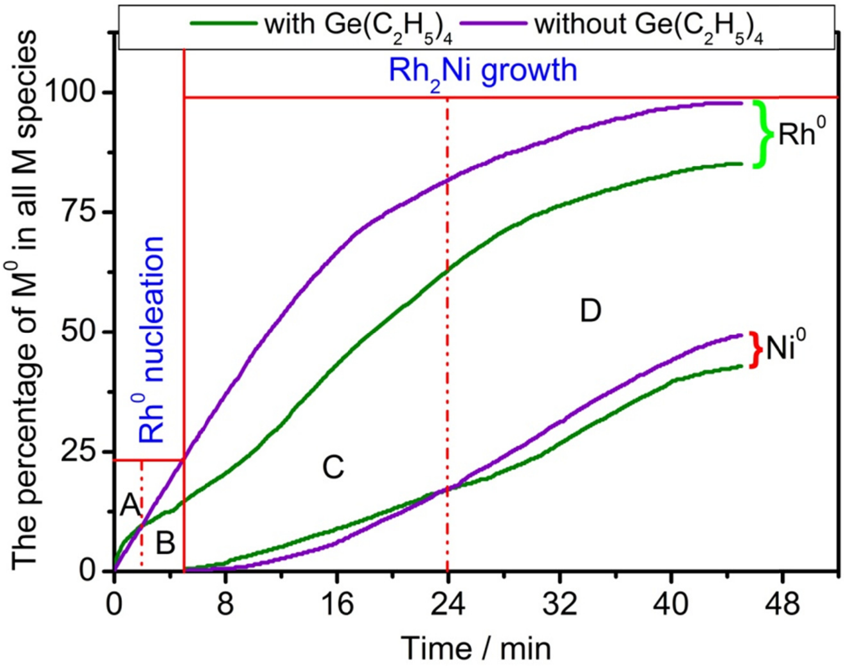

Figure S20. The Rh^0 and Ni^0 percentage in all Rh and Ni species obtained from the *in-situ* XPS measurement during the preparation process of Rh_2Ni NCs with or without the presence of $Ge(C_2H_5)_4$, respectively.

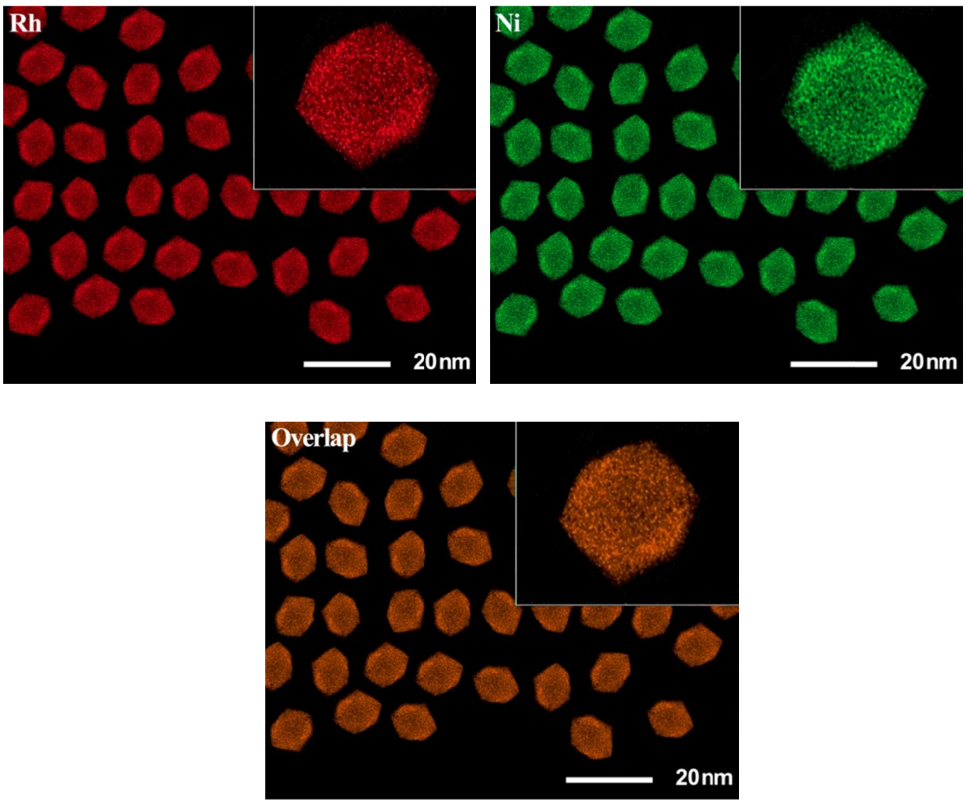

Figure S21. The elemental maps of the as-prepared Rh_2Ni trunked nanooctahedrons in this work.

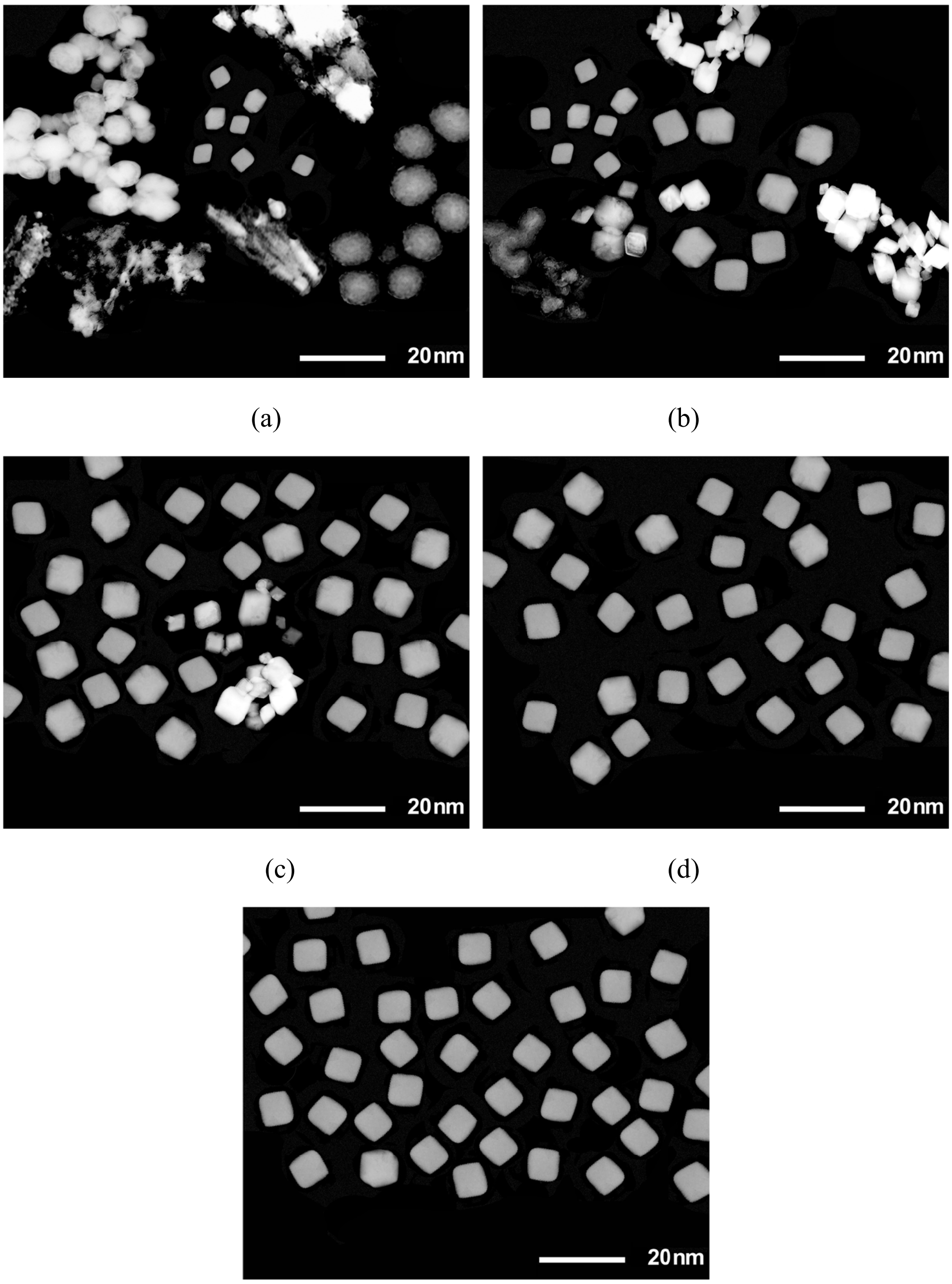

Figure S22. STEM images of Rh_2Ni synthesized by varying the amounts of 1-aminoheptadecane: (a) 0.01 mmol; (b) 0.025 mmol, (c) 0.05 mmol, (d) 0.075 mmol and (d) 0.1 mmol, respectively.

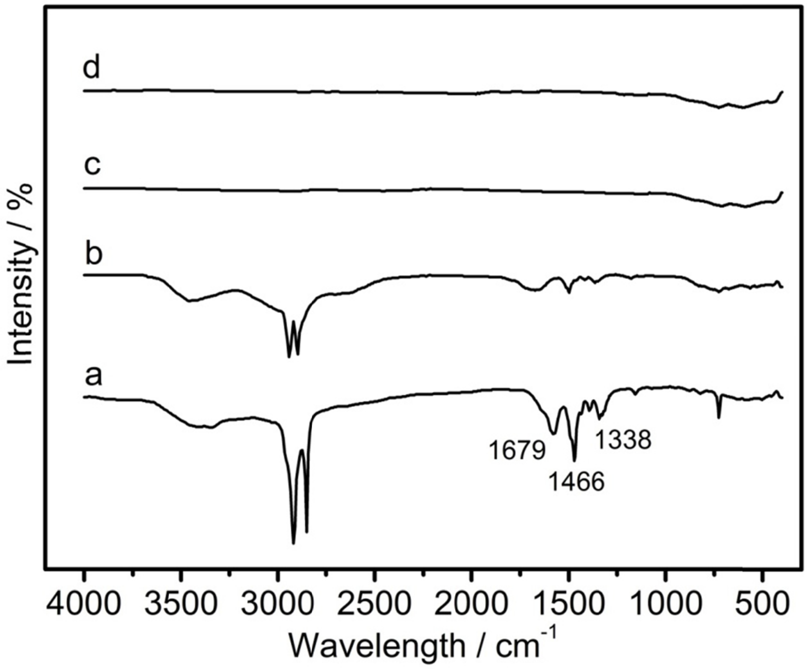

Figure S23. FT-IR spectra of (a) 1-aminoheptadecane; (b) the as-prepared Rh_2Ni nanocubes only washed with water; (c) the as-prepared Rh_2Ni nanocubes washed with ethanol; and (d) commercial Rh_2Ni NPs.

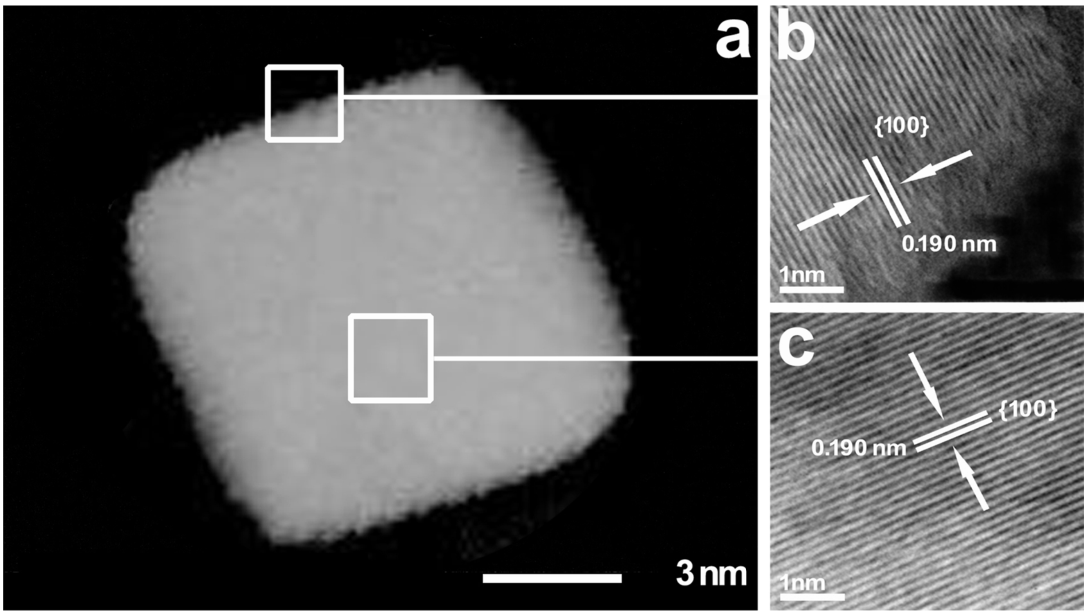

Figure S24. (a)The high resolution STEM (HR-STEM) image of a single Rh_2Ni nanocube; (b, c) Corresponding HR-STEM images of the regions marked in (a).

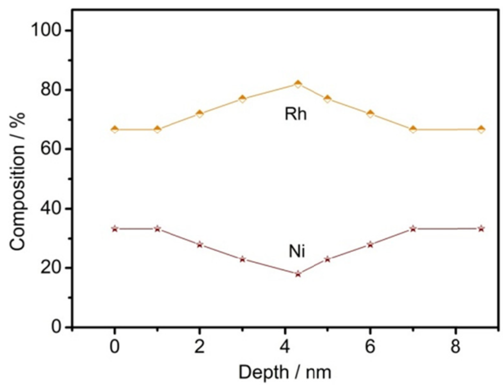

Figure S25. XPS Depth profile curves obtained using X-ray photoelectron spectroscopy of the as-prepared Rh_2Ni nanocubes in this work.

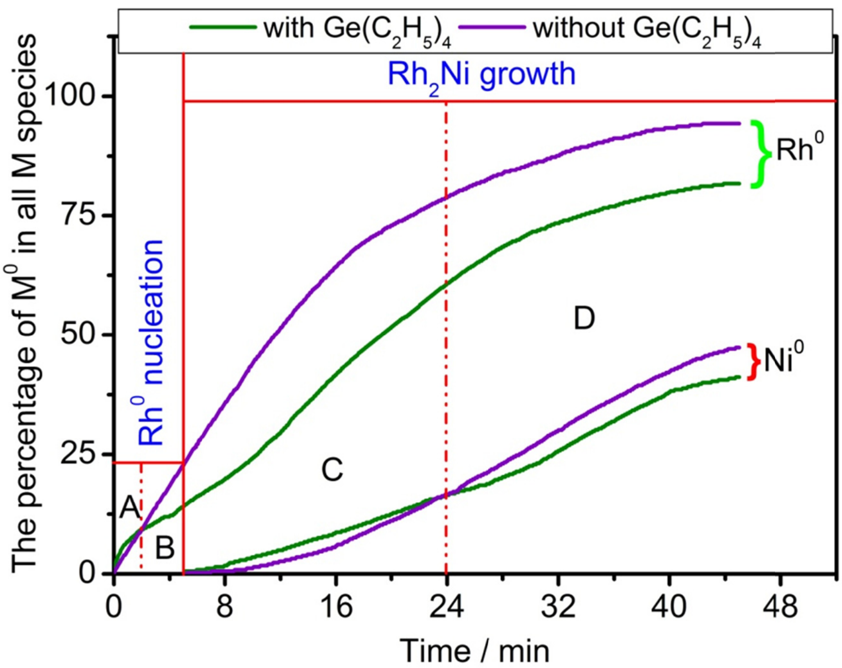

Figure S26. The Rh^0 and Ni^0 percentage in all Rh and Ni species obtained from the *in-situ* XPS measurement during the preparation process of Rh_2Ni NCs with or without the presence of $Ge(C_2H_5)_4$, respectively.

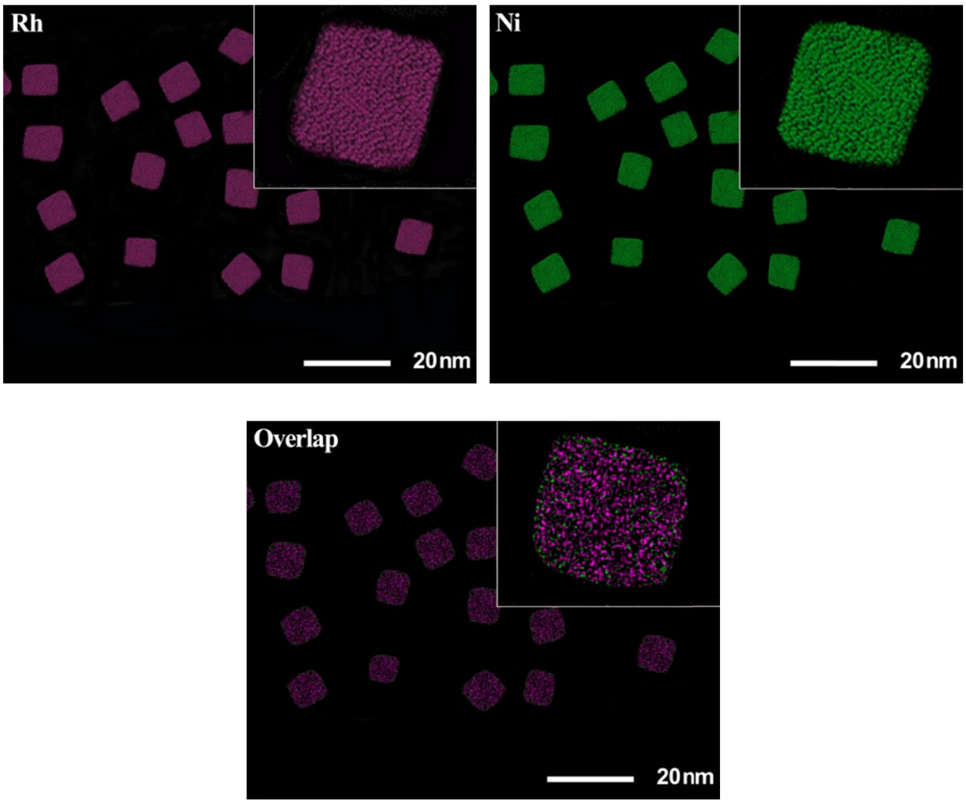

Figure S27. The elemental maps of the as-prepared Rh_2Ni nanocubes in this work.

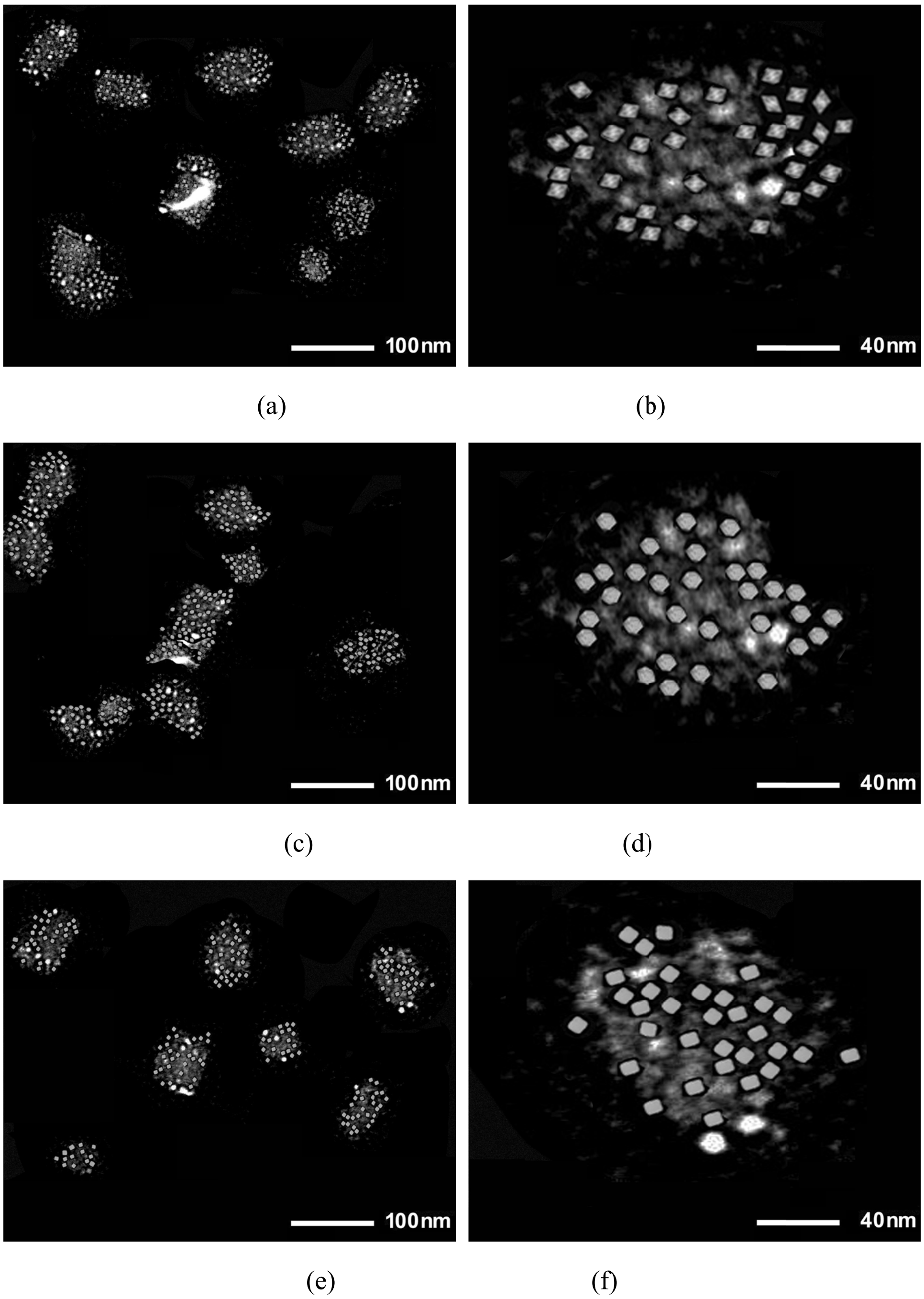

Figure S28. (a) STEM image and (b) enlarged STEM image of the 8.6 nm Rh_2Ni nanooctahedrons supported on carbon; (c) STEM image and (d) enlarged STEM image of the 8.6 nm Rh_2Ni truncated nanooctahedrons nanospheres supported on carbon; (e) STEM image and (f) enlarged STEM image of the 8.6 nm Rh_2Ni nanocubes supported on carbon.

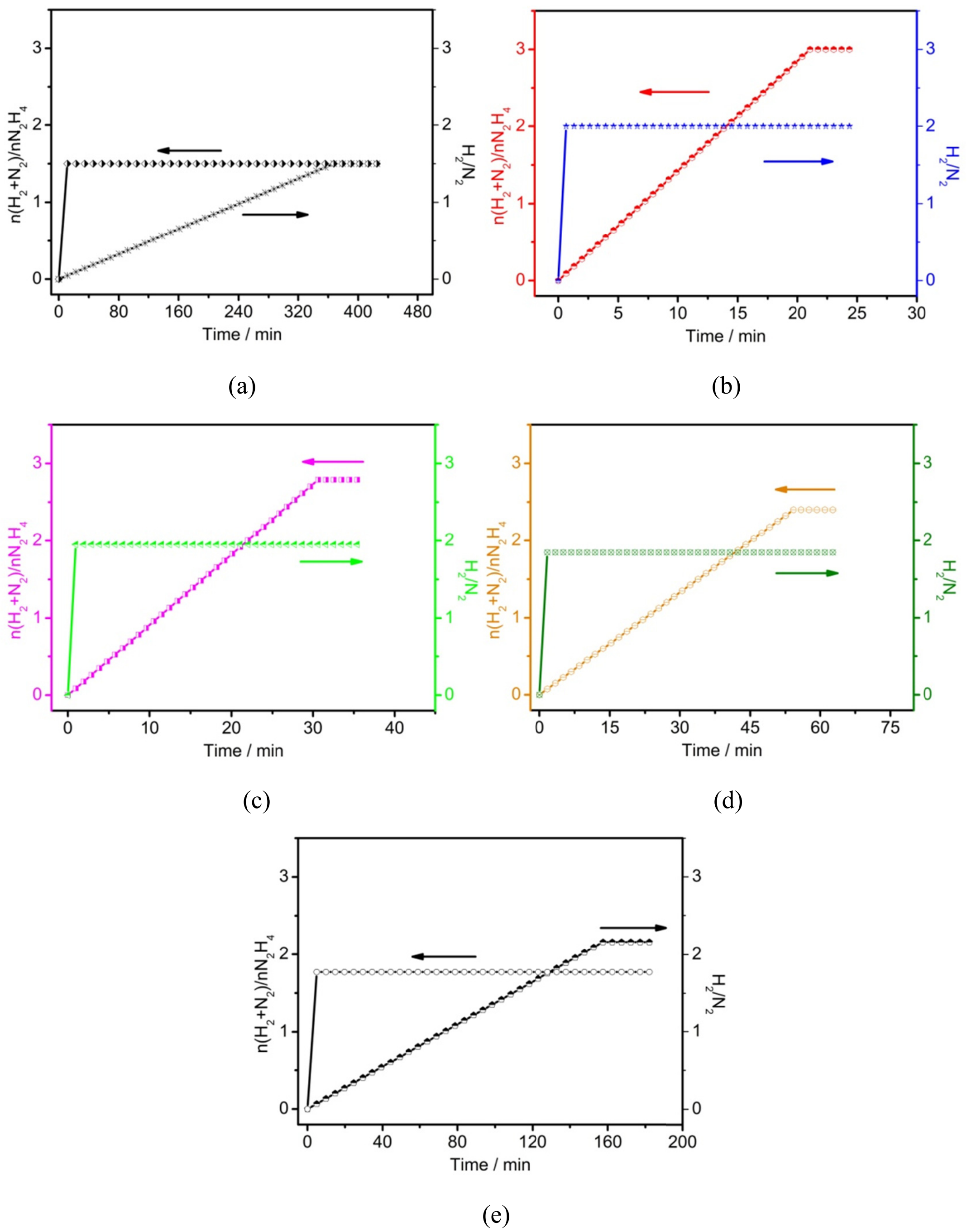

Figure S29. The $n(H_2 + N_2)/n(N_2H_4)$ and **H_2/N_2** molar ratio versus time for 0.297 mmol of surface "clean" (a) Rh nanooctahedrons, (b) Rh_2Ni nanooctahedrons, (c) Rh_2Ni truncated nanooctahedrons, (d) Rh_2Ni nanocubes and (e) Ni nanooctahedrons supported on 30 mg carbon during the decomposition of 100 mL of hydrazine in aqueous solution with a concentration of 0.49 mol L^{-1} at 293 K.

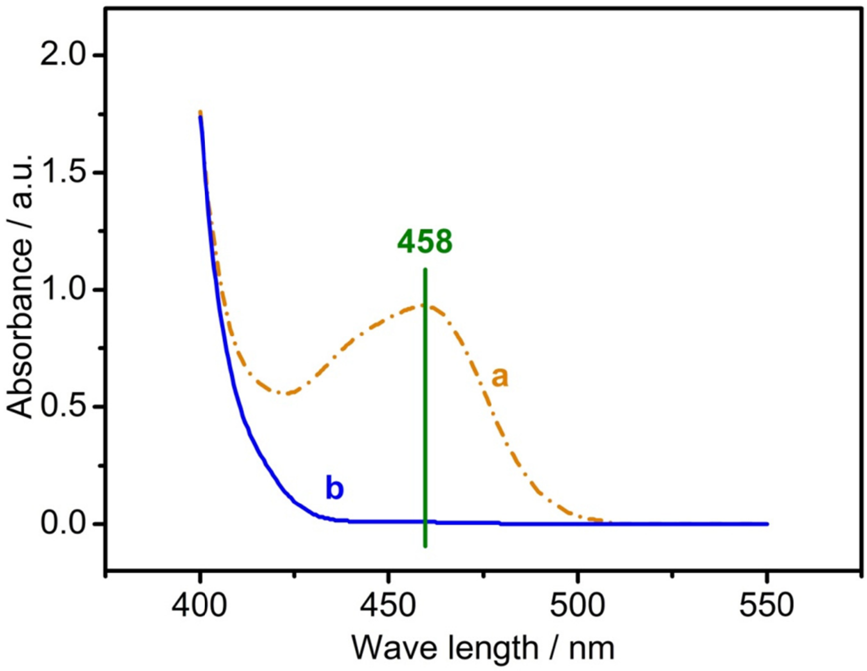

Figure S30. Typical UV-Vis spectra of hydrazine in aqueous solution (a) before and (b) after the completion of hydrazine decomposition reaction over surface “clean” Rh_2Ni or Rh or Ni NCs supported on carbon.

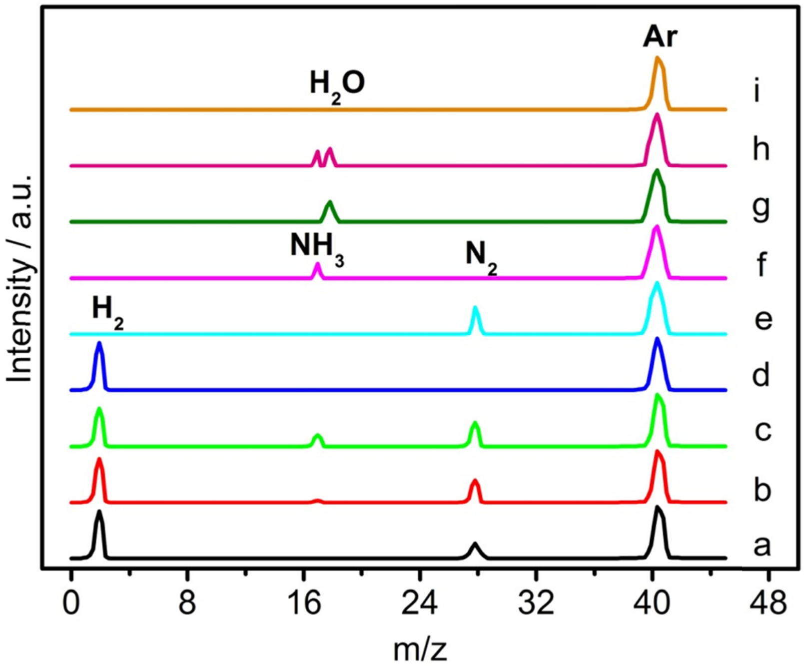

Figure S31. Mass spectral (MS) profile of (a) the gases released from the complete decomposition of hydrazine in aqueous solution at room temperature over surface "clean" Rh_2Ni nanooctahedrons/C, (b) the gases released from the complete decomposition of hydrazine in aqueous solution at room temperature over Rh_2Ni truncated nanooctahedrons/C, (c) the gases released from the complete decomposition of hydrazine in aqueous solution at room temperature over Rh_2Ni nanocubes/C; (d) H_2; (e)N_2; (f) NH_3; (g) H_2O; (h) NH_3+H_2O; and (i) carrier Ar.

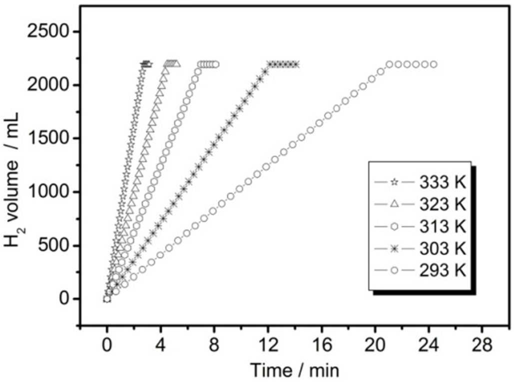

(a)

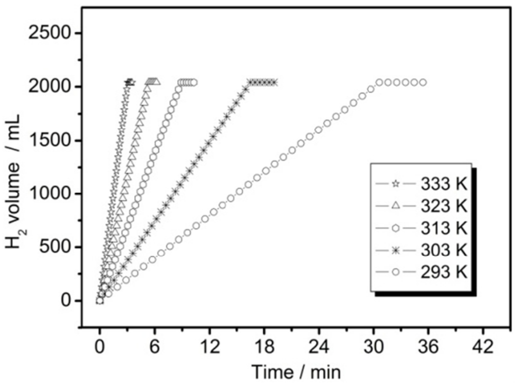

(b)

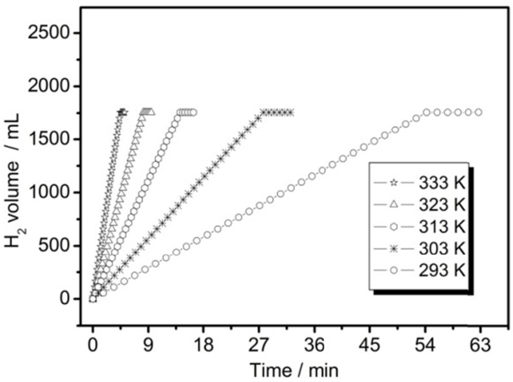

(c)

Figure S32. Plots of volume of hydrogen generated versus time during the hydrazine decomposition over 0.297 mmol of surface "clean" (a) Rh_2Ni nanooctahedrons, (b) Rh_2Ni truncated nanooctahedrons and (c) Rh_2Ni nanocubes supported on 30 mg carbon at different temperatures in the range 293 K–333 K ($[N_2H_4] = 0.49$ mol L^{-1}).

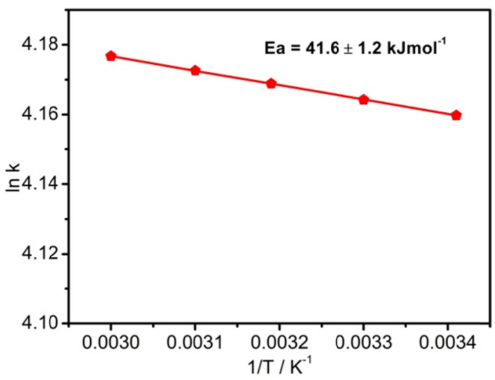

(a)

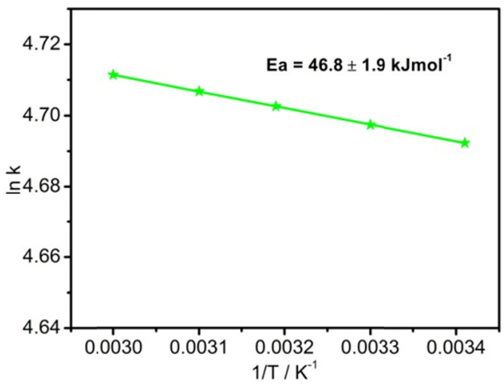

(b)

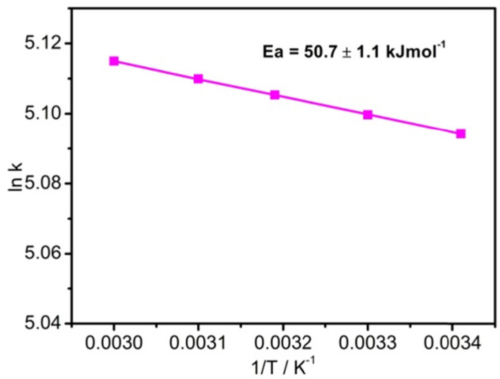

(c)

Figure S33. The plot of lnk versus 1/T during the hydrazine decomposition over 0.297 mmol of surface "clean" (a) Rh_2Ni nanooctahedrons, (b) Rh_2Ni truncated nanooctahedrons and (c) Rh_2Ni nanocubes supported on 30 mg carbon at different temperatures in the range 293 K–333 K ($[N_2H_4]$ = 0.49 mol L^{-1}).

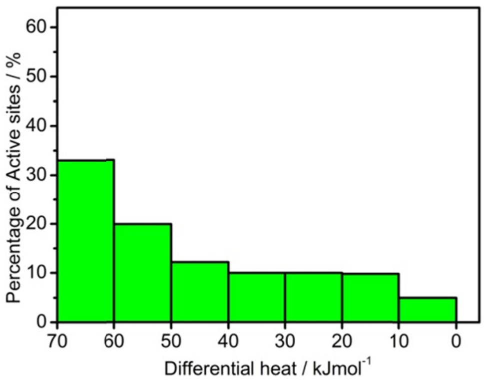

(a)

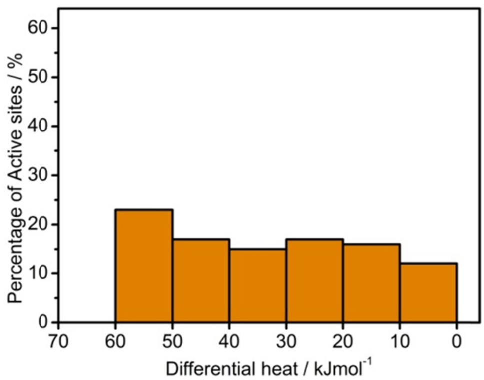

(b)

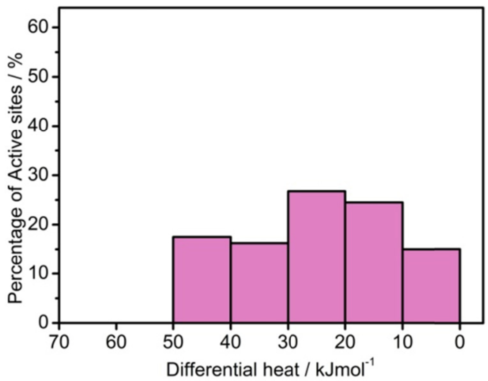

(c)

Figure S34. The differential heat of H_2 adsorption distribution histograms of surface “clean” (a) Rh_2Ni nanocubes, (b) Rh_2Ni truncated nanooctahedrons and (c) Rh_2Ni nanooctahedrons.

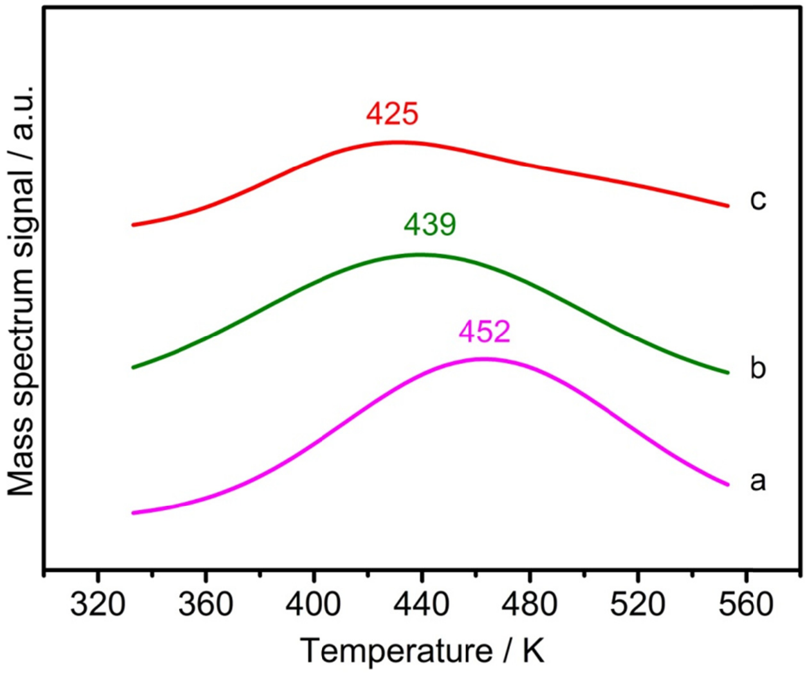

Figure S35. Mass spectra of H_2-TPD for surface "clean" (a) Rh_2Ni nanocubes, (b) Rh_2Ni truncated nanooctahedrons and (c) Rh_2Ni nanooctahedrons.

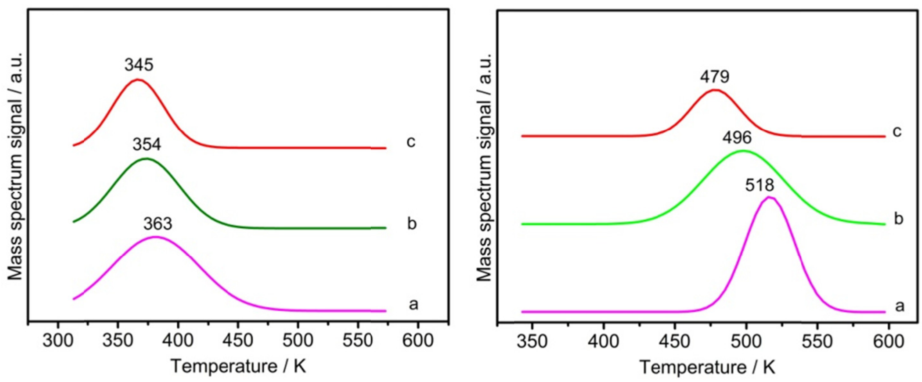

(A) (B)

Figure S36. Mass spectra of NH_3 TPD-MS for (A) NH_3 desorption signal and (B) N_2 desorption signal for surface "clean" (a) Rh_2Ni nanocubes, (b) Rh_2Ni truncated nanooctahedrons and (c) Rh_2Ni nanooctahedrons.

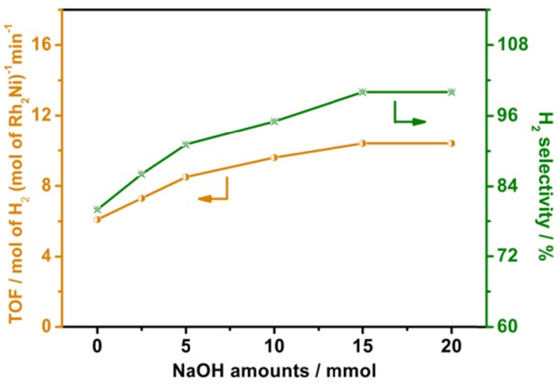

(a)

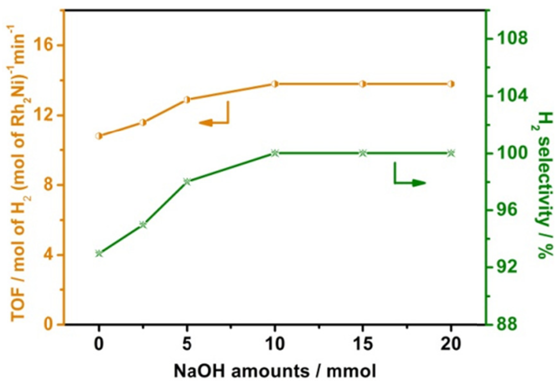

(b)

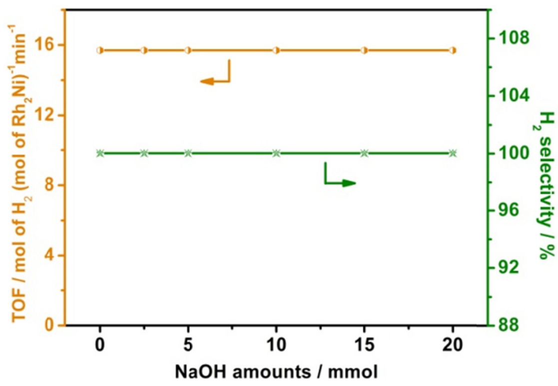

(c)

Figure S37. Plots of TOF value and hydrogen selectivity versus NaOH concentration over 0.297 mmol surface "clean" (a) Rh_2Ni nanocubes, (b) Rh_2Ni truncated nanooctahedrons and (c) Rh_2Ni nanooctahedrons supported on 30mg carbon at 293 K.

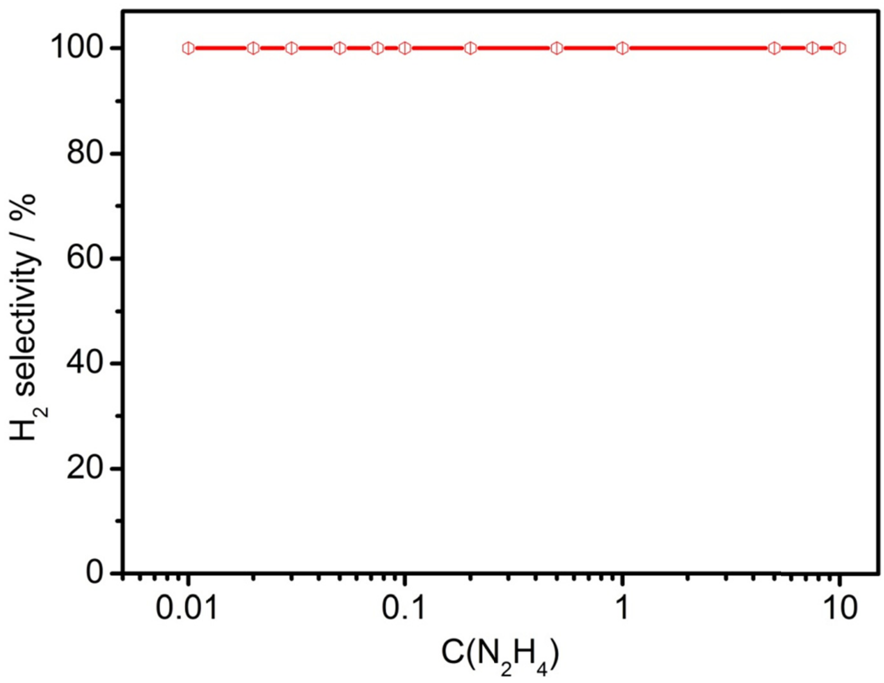

Figure S38. Hydrogen selectivity versus N_2H_4 concentrations for the decomposition of N_2H_4 over 0.297 mmol surface "clean" Rh_2Ni nanooctahedrons supported on 30mg carbon at 293 K.

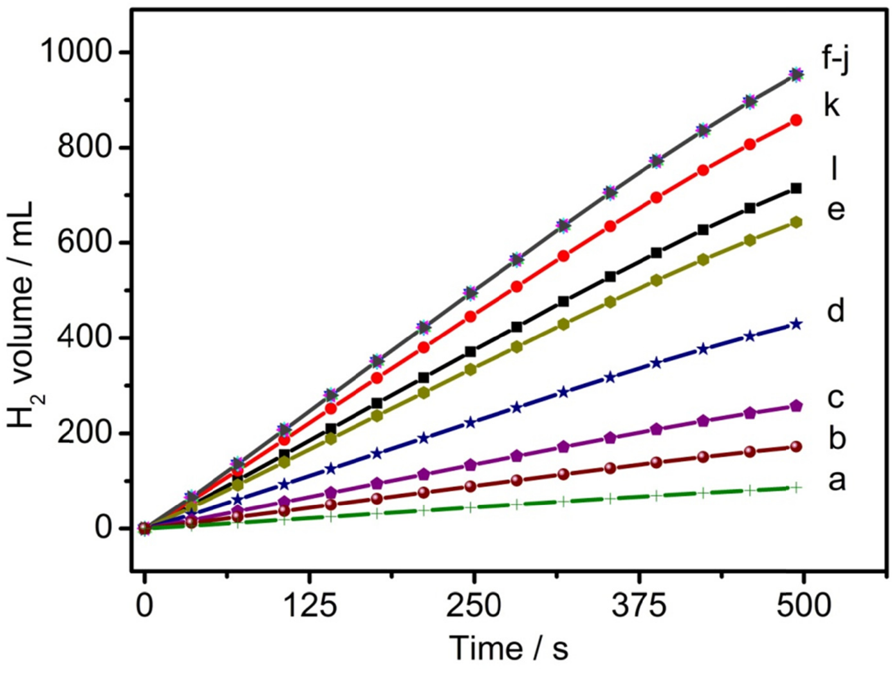

Figure S39. Hydrogen released from 20mL N_2H_4 solution with different concentrations (a) 0.01, (b) 0.02, (c) 0.03, (d) 0.05, (e) 0.075, (f) 0.1, (g) 0.2, (h) 0.5, (i) 1, (j) 5, (k) 7.5 and(l) 10.0molL^{-1} in the presence of 0.297 mmol surface "clean" Rh_2Ni nanooctahedrons supported on 30mg carbon at 293 K.

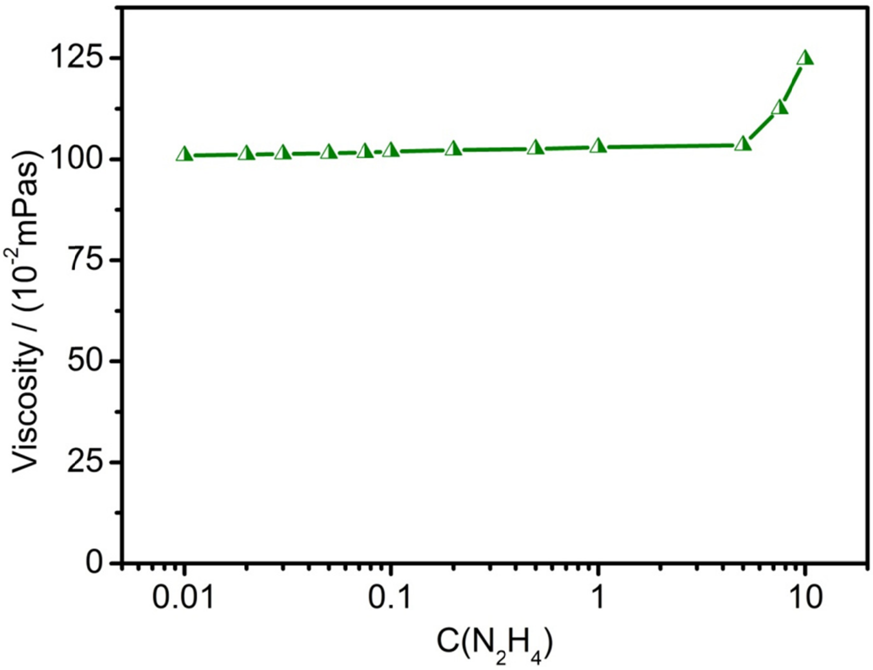

Figure S40. Viscosity versus N_2H_4 concentrations at 293 K.

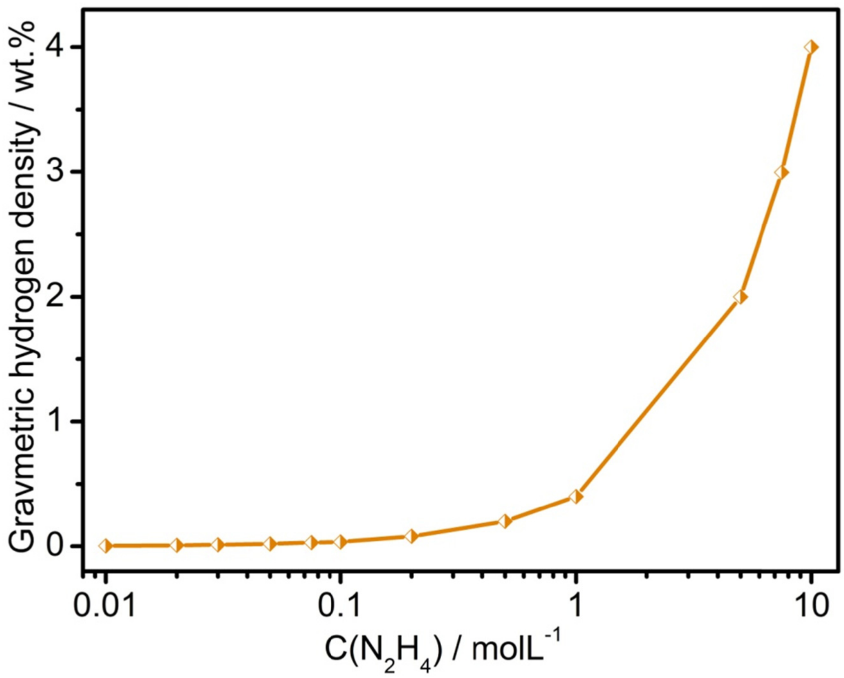

Figure S41. Solution gravimetric hydrogen densities versus N_2H_4 concentrations for the decomposition of N_2H_4 over 0.297 mmol surface "clean" Rh_2Ni nanooctahedrons supported on 30mg carbon at 293 K.

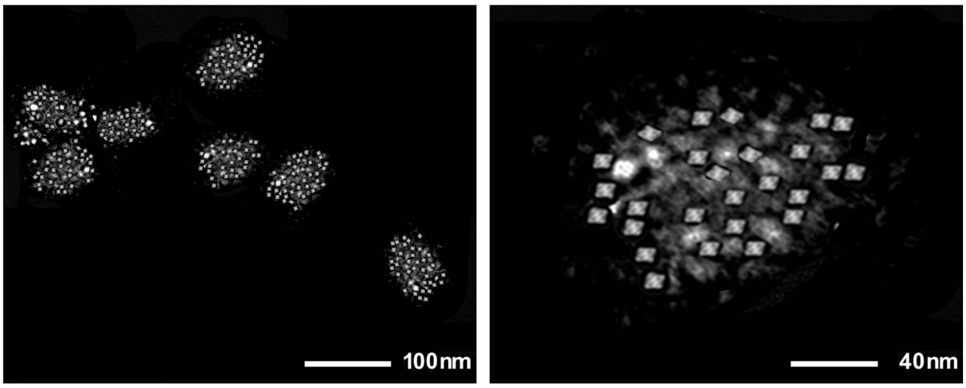

(a) (b)

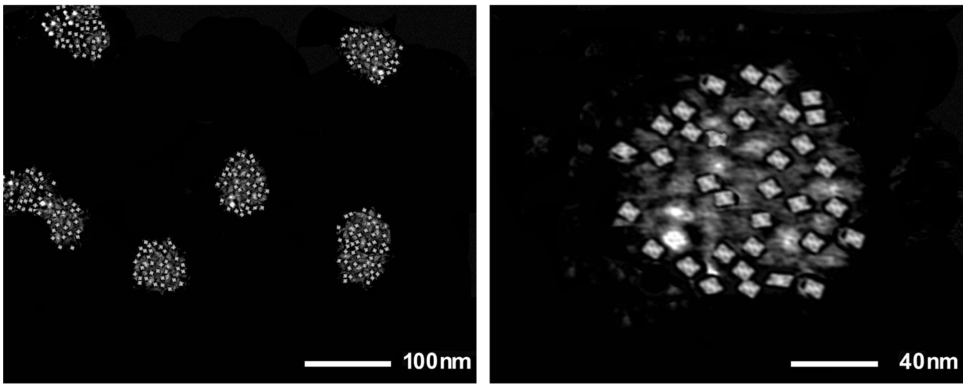

(c) (d)

Figure S42. (a) STEM image and (b) enlarged STEM image of the deactivated Rh_2Ni nanooctahedrons/C; (c) STEM image and (d) enlarged STEM image of the deactivated Rh_2Ni nanooctahedrons/C after reactivation by solution plasma process.

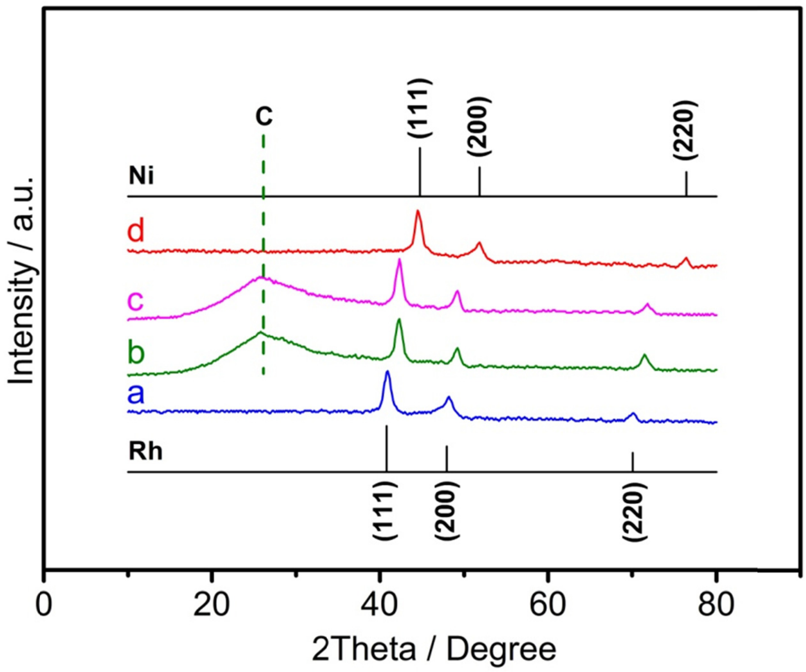

Figure S43. XRD profiles of (a) Rh nanooctahedrons; (b) the deactivated Rh_2Ni nanooctahedrons/C; (c) the deactivated Rh_2Ni nanooctahedrons /C after reactivation by solution plasma process; (d) Ni nanooctahedrons.

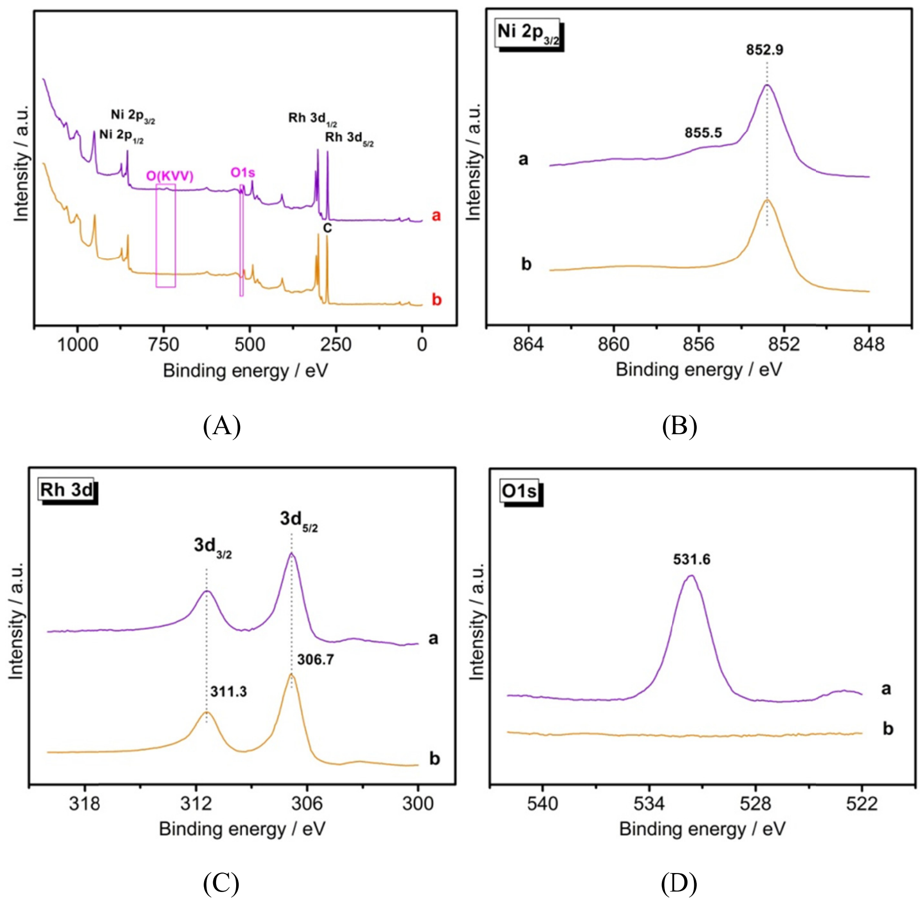

Figure S44. *in-situ* (A) Overall XPS spectra; (B) Ni2p3/2 XPS spectra; (C) Rh 3d XPS spectra; and (D) O1s XPS spectra of the deactivated Rh_2Ni nanooctahedrons /C (a) before reactivation and (b) after reactivation by solution plasma process.

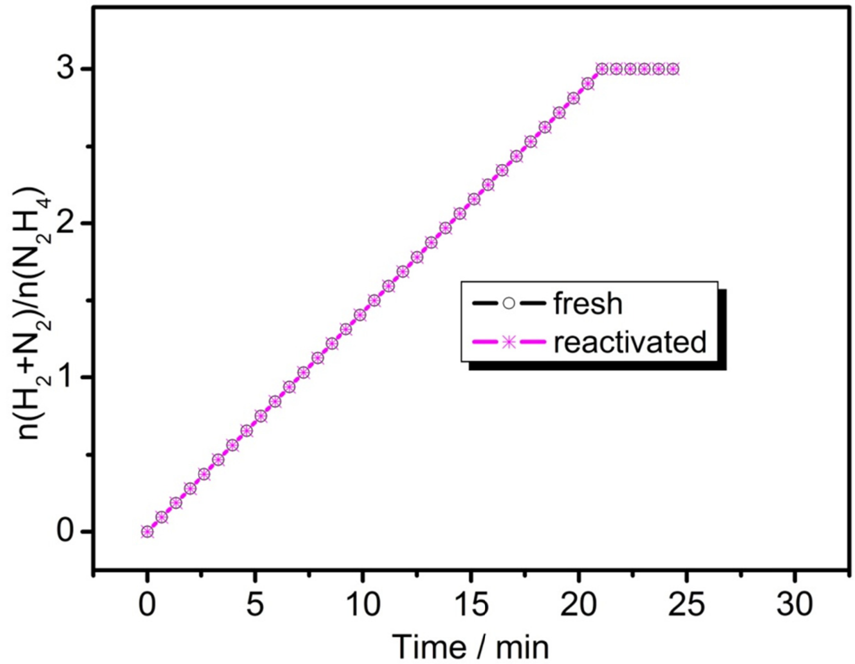

Figure S45. Time profiles for decomposition of hydrazine in aqueous solution in the presence (a) fresh and (b) reactivated Rh_2Ni nanooctahedrons /C

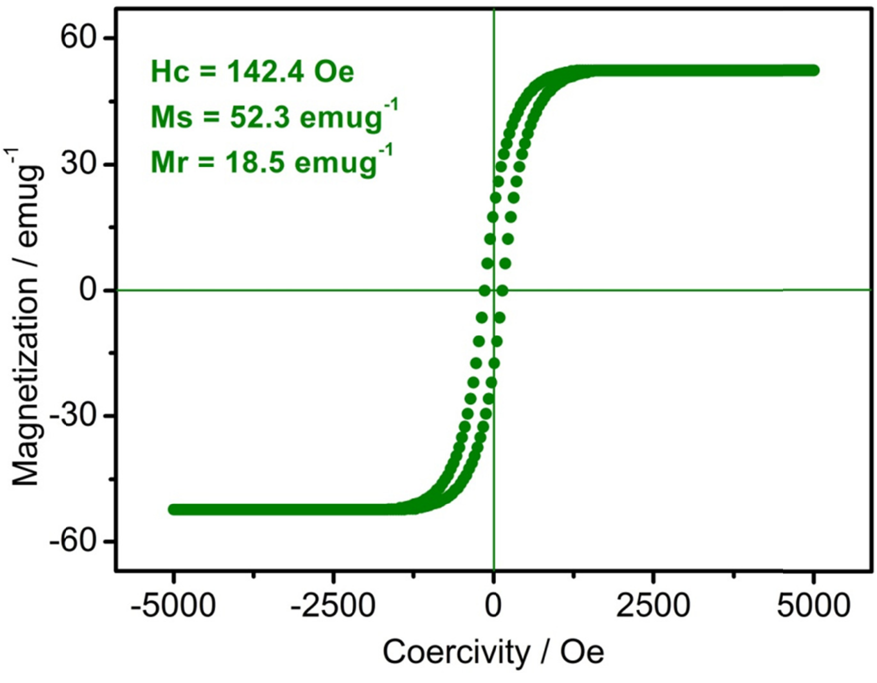

Figure S46. Hysteresis loop and magnetic properties of Ni nanooctahedrons.

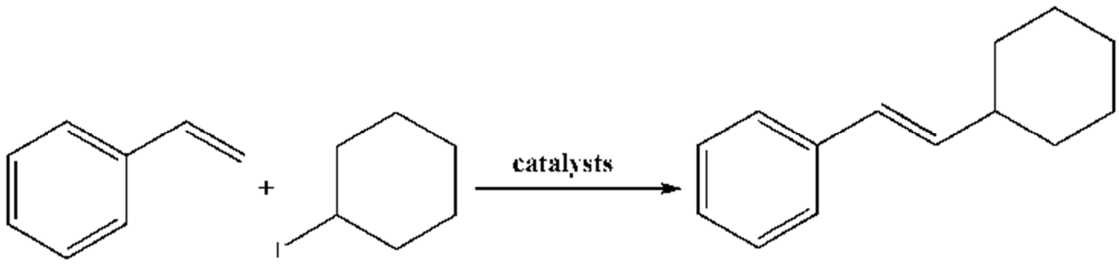

Figure S47. Heck-type coupling reaction between cyclohexyliodide and styrene over catalysts.

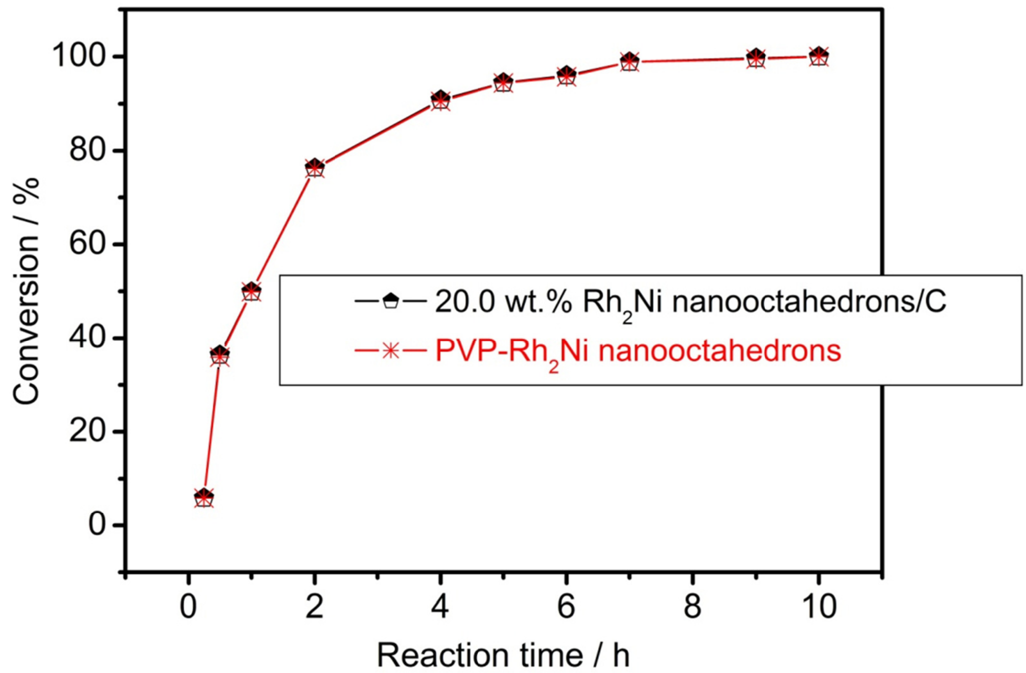

(a)

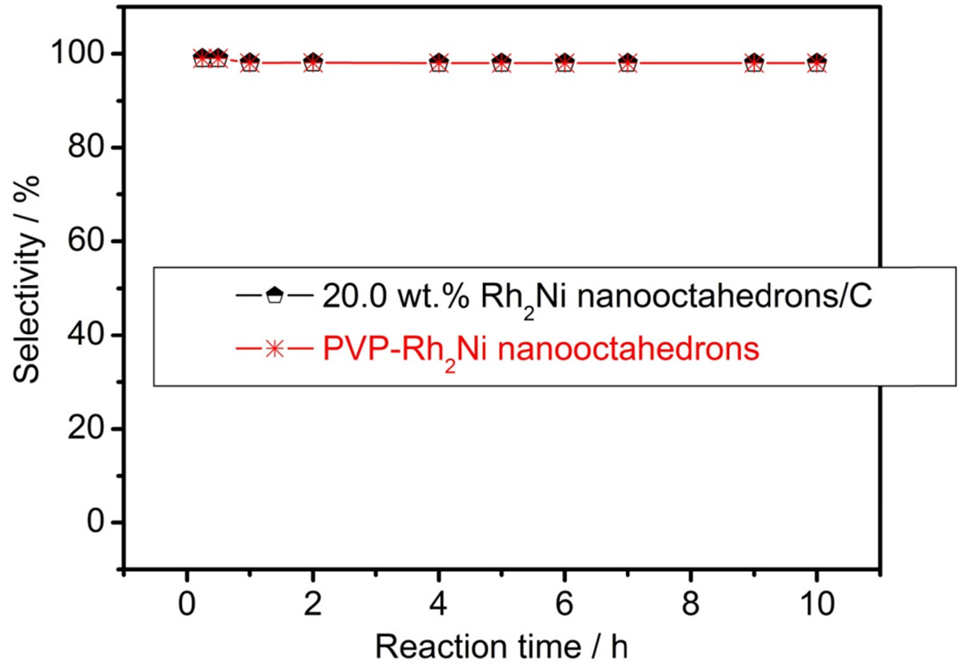

(b)

Figure S48. Dependency of the cyclohexyliodide conversion and the (E)-(2-cyclohexylvinyl)benzene selectivity on reaction time over 20.0 wt.% Rh_2Ni nanooctahedrons/C and PVP-Rh_2Ni nanooctahedrons. Reaction conditions: a catalyst containing 10 mg Rh_2Ni, cyclohexyliodide (5.0 mmol), alkenes (6.0 mmol), Na_2CO_3 (7.5 mmol), DMF (10 mL), T = 353 K, stirring rate = 800 rpm.

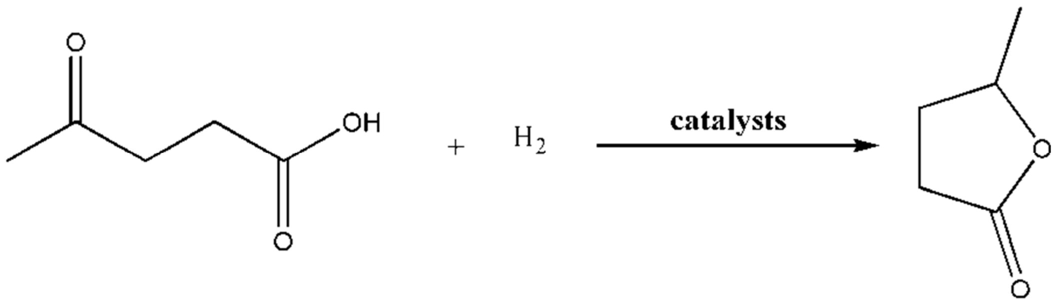

Figure S49. Hydrogenation of LA to GAL over catalysts

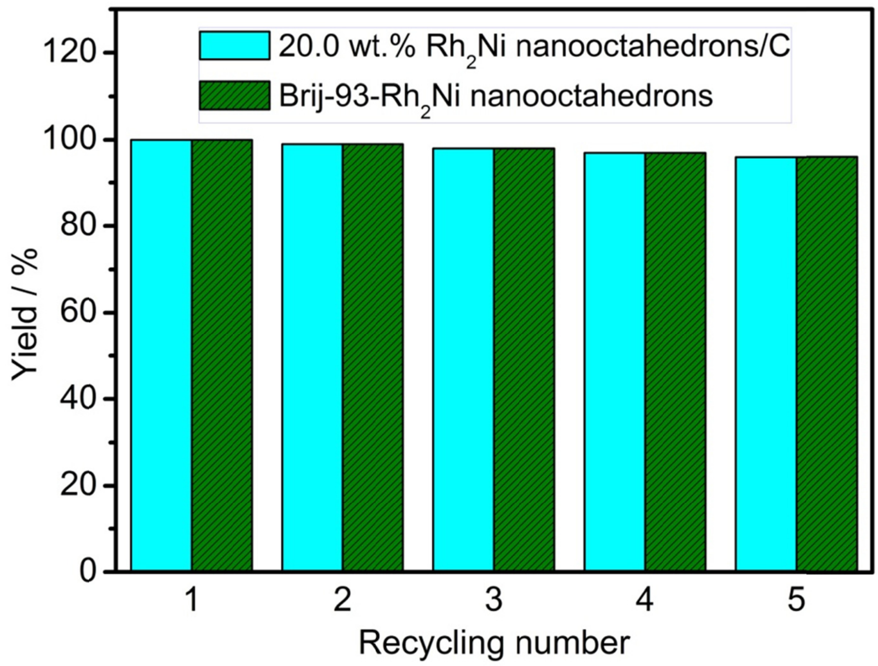

Figure S50. Recycling tests of 20.0 wt.% Rh_2Ni nanooctahedrons/C and Brij-93-Rh_2Ni nanooctahedrons for LA hydrogenation to GAL. Reaction conditions: catalyst containing 10 mg of Rh_2Ni nanooctahedrons, 20 mmol of LA, 50 mL of n-dodecane, PH_2 = 4.2 MPa H_2, T = 413 K, reaction time = 2 h, stirring rate = 1100 rpm.